IMA Journal of Numerical Analysis (2014) **34**, 1625–1653
doi:10.1093/imanum/drt049
Advance Access publication on October 28, 2013

A posteriori error estimates for mixed finite element and finite volume methods for problems coupled through a boundary with nonmatching grids

T. Arbogast
Department of Mathematics, University of Texas, Austin, TX, USA
arbogast@math.utexas.edu

D. Estep*
Department of Statistics, Colorado State University, Fort Collins, CO 80523, USA
*Corresponding author: estep@stat.colostate.edu

and

B. Sheehan and S. Tavener
Department of Mathematics, Colorado State University
brendansheehan6@gmail.com

[Received on 9 September 2012; revised on 25 August 2013]

The primary purpose of this paper is to compare the accuracy and performance of two numerical approaches to solving systems of partial differential equations. These equations are posed on adjoining domains sharing boundary conditions on a common boundary interface in the important case when the meshes used on the two domains are nonmatching across the interface. The first, widely used approach is based on a finite volume method employing *ad hoc* projections to relate approximations on the two domains across the interface. The second approach uses the mathematically founded mortar mixed finite element method. To quantify the performance, we use a goal-oriented *a posteriori* error estimate that quantifies various aspects of discretization error to the overall error. While the performance difference may not be a surprise in some cases, we believe that there is a perception in a part of the scientific community concerned with multiphysics systems that if the solution is smooth near the interface, then there is little effect from varying the coupling technique. We find that, on the contrary, the error associated with *ad hoc* coupling approaches may be large in practical situations. Moreover, we also show that mortar methods can be used with black-box component solvers, thus permitting an efficient and practical implementation also within legacy codes.

Keywords: mortar methods; *a posteriori* error estimate; coupled elliptic problems; heterogeneous domain decomposition; geometric coupling.

1. Introduction

An important class of multiphysics problems have a structure in which one physical process dominates in one subdomain of the problem domain, while a second physical process dominates in a neighbouring subdomain. The solutions are coupled by continuity of state and continuity of normal flux through a shared boundary between the subdomains. Examples include general problems of the heterogeneous domain decomposition type (Quarteroni *et al.*, 1992; Bernardi *et al.*, 1994; Gaiffe *et al.*, 2002), core–edge plasma simulations of a tokamak fusion experiment (Cary *et al.*, 2008, 2010) and conjugate heat transfer between a fluid and solid object (Estep *et al.*, 2008, 2009b, 2010).

In such situations, it is common to encounter significant differences in scales of behaviour in the two subdomains. This in turn suggests the use of different discretization grids. However, this introduces the

problem of interpreting the meaning of coupling state and flux values through the common boundary in the discretization, since exact pointwise matching is no longer possible.

Confounding this issue are the practical difficulties of solving the large linear and nonlinear discrete systems associated with computing numerical solutions and the common situation in which two different codes are used to solve the two subdomain problems. These difficulties are generally tackled by employing some form of iterative approach that involves the sequential solution of the subdomain problems. The particular properties of the discretizations used for each component problem, the choice of iterative solution method and high performance computational considerations all have a large impact on the way in which state and flux values are passed across the common interface.

In this paper, we investigate the accuracy of two approaches to computing the coupling values in the situation in which the discretization grids in the two subdomains do not match at the interface. The analysis is carried out for the closely related mixed finite element and cell-centred finite volume methods. The two approaches are (1) the mortar element approach (Brezzi & Fortin, 1991; Roberts & Thomas, 1991; Arbogast *et al.*, 2000, 2007; Ben Belgacem, 2000; Ganis & Yotov, 2009), which uses a rigorous variational formulation to define a weak sense of coupling and (2) a 'geometric' approach that employs various *ad hoc* extrapolation and averaging methods. The use of mortar elements is proved to be optimally convergent on nonmatching grids, provided the finite element space used for the interface variables consists of piecewise polynomials of one degree higher than the trace along the interface of the finite element space used to approximate the flux within the subdomains (Arbogast *et al.*, 2000). Nonetheless, while mortar elements are well known in some application domains, e.g., flow in porous media, they are not widely employed for multiphysics problems. Rather, various 'geometric' techniques are used in most practical settings, especially in situations in which one or more of the components are solved with legacy 'black-box' codes. This second approach is often rationalized using a combination of *ad hoc* formal stability and/or accuracy arguments combined with high performance computing expediences. Moreover, in the situation in which legacy codes are used to solve either component, there is little choice because of the very considerable investment that would be required to replace these codes.

We are not arguing for or against either mortar elements or 'geometric' approaches. Rather, we address two issues: (1) what effect do these coupling approaches have on the accuracy of specified quantities of interest? and (2) in each case, quantify the relative contributions of various aspects of discretization to the error in the computed information. The tool we use to address these issues is an adjoint-based *a posteriori* error estimate (Estep *et al.*, 2000; Becker & Rannacher, 2001; Giles & Suli, 2002; Wheeler & Yotov, 2005; Estep *et al.*, 2009a; Hansbro & Larson, 2011; Pencheva *et al.*, 2013). This goal-oriented estimate accurately quantifies various contributions to the overall error. In particular, the estimate distinguishes contributions specifically arising from the mismatched grids and the way in which the coupled information is approximated. We identify, through numerical examples, cases in which the geometric projections are the dominant source of error by one to two orders of magnitude.

The remainder of this paper is organized as follows. Section 2 introduces the differential equation and the details of the two discrete methods. Section 3 derives the *a posteriori* error estimate. Section 4 contains the numerical experiments. Section 5 discusses computational logistics related to iterative solvers, and a brief conclusion is given in Section 6.

2. Definition of the problem and discretization methods

We define the coupled problem with a common interface and then describe the finite element and finite volume discretizations. We employ the well-known equivalence between finite volume methods and the mixed finite element method (Russell & Wheeler, 1983; Weiser & Wheeler, 1988) to recast everything in the finite element framework. This greatly eases the derivation of *a posteriori* error estimates and provides a systematic framework for describing geometric approaches to computing coupling values.

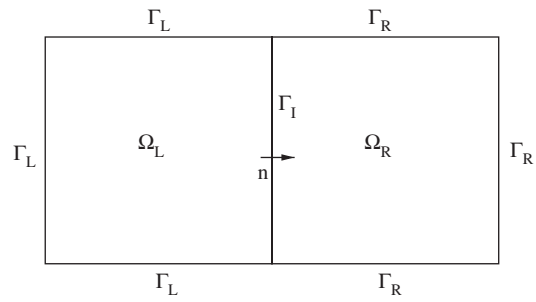

FIG. 1. Subdomains, boundaries and definition of the normal n on the interface.

2.1 *The differential equation*

The differential equation (2.1–2.3) consists of a system of second-order elliptic partial differential equations (PDEs) in two spatial dimensions. The system is posed on a rectangular domain Ω consisting of two nonoverlapping rectangular subdomains, Ω_L on the left-hand side and Ω_R on the right-hand side, that share a common interface Γ_I and whose union forms the entire domain, as shown in Fig. 1. The unit normal vector n is defined to point from left to right on Γ_I and is an outward-pointing normal on $\Gamma_L = \partial\Omega_L \setminus \Gamma_I$ and $\Gamma_R = \partial\Omega_R \setminus \Gamma_I$. For simplicity of presentation, we assume Dirichlet boundary conditions on $\partial\Omega$, the external boundaries of the domain. The results extend to problems with Neumann conditions on part of the boundary in a straightforward way.

For a diffusion function a, split as $a_L \in W^{1,\infty}(\Omega_L)$ and $a_R \in W^{1,\infty}(\Omega_R)$, source function f, split as $f_L \in L^2(\Omega_L)$ and $f_R \in L^2(\Omega_R)$, and boundary data g, split as $g_L \in H^{3/2}(\Gamma_L)$ and $g_R \in H^{3/2}(\Gamma_R)$, the coupled system is

$$\begin{cases} a_L^{-1}\boldsymbol{u}_L + \nabla p_L = 0, & (x,y) \in \Omega_L, \\ \nabla \cdot \boldsymbol{u}_L = f_L, & (x,y) \in \Omega_L, \\ p_L = g_L, & (x,y) \in \Gamma_L, \end{cases} \tag{2.1}$$

$$\begin{cases} a_R^{-1}\boldsymbol{u}_R + \nabla p_R = 0, & (x,y) \in \Omega_R, \\ \nabla \cdot \boldsymbol{u}_R = f_R, & (x,y) \in \Omega_R, \\ p_R = g_R, & (x,y) \in \Gamma_R, \end{cases} \tag{2.2}$$

$$\begin{cases} \xi \equiv p_L = p_R, & (x,y) \in \Gamma_I, \\ \boldsymbol{n} \cdot (\boldsymbol{u}_L - \boldsymbol{u}_R) = 0, & (x,y) \in \Gamma_I, \end{cases} \tag{2.3}$$

where we assume that the diffusion matrices, a_L and a_R, are functions of space multiplied by the identity matrix, i.e.,

$$a_L = \begin{bmatrix} D_L(x,y) & 0 \\ 0 & D_L(x,y) \end{bmatrix}, \quad a_R = \begin{bmatrix} D_R(x,y) & 0 \\ 0 & D_R(x,y) \end{bmatrix}, \tag{2.4}$$

with $D_i \in W^{1,\infty}(\Omega_i)$, $i = L, R$, and $\min_{(x,y)\in\bar{\Omega}_i} D_i(x,y) \geqslant D_0 > 0$, so a_i is invertible and uniformly coercive for $i = L, R$. Note that we have defined ξ as the common interface pressure in (2.3).

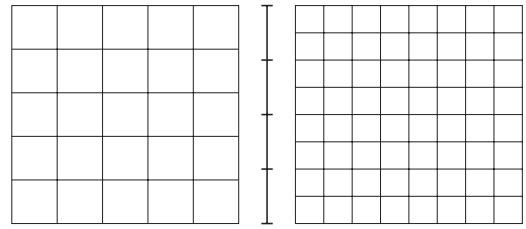

FIG. 2. Example grid shown separated, from left to right, into the part on Ω_{L}, Γ_{I} and Ω_{R}.

2.2 *Mixed finite element mortar discretization*

The mortar finite element discretization was developed precisely for the situation presented by the discretization of (2.1–2.3) using two different grids in the two different subdomains. We assume that each subdomain is discretized by a (logically) rectangular finite element grid. Lagrange multipliers are introduced on the interface boundary to provide a weak formulation of the pressure coupling conditions. Since the grids are different on the two sides of the interface, the Lagrange multiplier space cannot be the normal trace of the velocity space. So, we introduce a mortar finite element space on the interface (Arbogast *et al.*, 2000, 2007; Bernardi *et al.*, 2005). As shown in Arbogast *et al.* (2000), the method is optimally convergent and has several other desirable convergence properties if the boundary space has one order higher approximability than the normal trace of the velocity space. The same order of convergence is obtained for both continuous or discontinuous piecewise polynomials in the mortar space. In our discretization, we choose an interface grid that has one cell for every two cells in the finer of the two subdomain grids. Figure 2 shows the arrangement for a 5×5 grid next to an 8×8 grid. (Note that our convention is that the finer grid is always used in the right-hand subdomain.)

We use standard L^2 inner product notation, i.e., for functions F and G defined on Ω, split as above,

$$(F_i, G_i) = \int_{\Omega_i} F_i(x,y) G_i(x,y)\,\mathrm{d}x\,\mathrm{d}y, \quad i = \mathrm{L}, \mathrm{R},$$

and for functions defined on the boundaries, we similarly define

$$\langle F, G\rangle_{\Gamma_i} = \int_{\Gamma_i} FG\,\mathrm{d}s, \quad i = \mathrm{L}, \mathrm{I}, \mathrm{R}.$$

The mixed finite element (mortar) method starts with the following continuous weak formulation. Find $p_i \in W_i = L^2(\Omega_i)$, $\boldsymbol{u}_i \in \boldsymbol{V}_i = H(\mathrm{div}; \Omega_i)$, $\xi \in \Lambda = H^{1/2}(\Gamma_{\mathrm{I}})$, $i = \mathrm{L}, \mathrm{R}$, satisfying

$$\begin{aligned}
&(a_{\mathrm{L}}^{-1}\boldsymbol{u}_{\mathrm{L}}, \boldsymbol{v}_{\mathrm{L}}) - (p_{\mathrm{L}}, \nabla\cdot\boldsymbol{v}_{\mathrm{L}}) + \langle \xi, \boldsymbol{n}\cdot\boldsymbol{v}_{\mathrm{L}}\rangle_{\Gamma_{\mathrm{I}}} = -\langle g_{\mathrm{L}}, \boldsymbol{n}\cdot\boldsymbol{v}_{\mathrm{L}}\rangle_{\Gamma_{\mathrm{L}}},\\
&(\nabla\cdot\boldsymbol{u}_{\mathrm{L}}, w_{\mathrm{L}}) = (f_{\mathrm{L}}, w_{\mathrm{L}}),\\
&(a_{\mathrm{R}}^{-1}\boldsymbol{u}_{\mathrm{R}}, \boldsymbol{v}_{\mathrm{R}}) - (p_{\mathrm{R}}, \nabla\cdot\boldsymbol{v}_{\mathrm{R}}) - \langle \xi, \boldsymbol{n}\cdot\boldsymbol{v}_{\mathrm{R}}\rangle_{\Gamma_{\mathrm{I}}} = -\langle g_{\mathrm{R}}, \boldsymbol{n}\cdot\boldsymbol{v}_{\mathrm{R}}\rangle_{\Gamma_{\mathrm{R}}},\\
&(\nabla\cdot\boldsymbol{u}_{\mathrm{R}}, w_{\mathrm{R}}) = (f_{\mathrm{R}}, w_{\mathrm{R}}),\\
&\langle \boldsymbol{n}\cdot(\boldsymbol{u}_{\mathrm{L}} - \boldsymbol{u}_{\mathrm{R}}), \nu\rangle_{\Gamma_{\mathrm{I}}} = 0,
\end{aligned} \tag{2.5}$$

for all $(w_i, \boldsymbol{v}_i, \nu) \in (W_i, \boldsymbol{V}_i, \Lambda)$, $i = \mathrm{L}, \mathrm{R}$.

To discretize, we use the lowest-order Raviart–Thomas finite element space (RT0), in which the discrete scalar unknown p^h is approximated as a constant over each cell, and the components of the discrete vector $\boldsymbol{u}^h$ are approximated by functions that are piecewise linear in one spatial dimension and constant in the other (Bernardi *et al.*, 2005; Estep *et al.*, 2009a). The discrete interface unknown, ξ^h, is represented by piecewise discontinuous linears on the interface grid cells (Arbogast *et al.*, 2000, 2007). The test functions in the discretization of the weak formulation of (2.5) corresponding to w, $\boldsymbol{v}$ and ν are restricted to these same spaces. To be precise, for a finite element partition Δ of $[a,b]$ and for $r=0,1,2,\ldots,\ q=-1,0,1,\ldots$, we define the piecewise polynomial space

$$\mathscr{M}_q^r(\Delta)=\{v\in C^q([a,b]):\ v \text{ is a polynomial of degree } \leqslant r \text{ on each subinterval of } \Delta\}.$$

When $q=-1$, the functions are discontinuous. The space of continuous piecewise bilinear functions is the tensor product $\mathscr{M}_0^1(\Delta_x)\otimes\mathscr{M}_0^1(\Delta_y)$. The RT0 discrete spaces are

$$\begin{aligned}
W_i^h &= \mathscr{M}_{-1}^0(\Delta_{x,i})\otimes\mathscr{M}_{-1}^0(\Delta_{y,i}), \quad i=\mathrm{L},\mathrm{R},\\
\boldsymbol{V}_i^h &= [\mathscr{M}_0^1(\Delta_{x,i})\otimes\mathscr{M}_{-1}^0(\Delta_{y,i})]\times[\mathscr{M}_{-1}^0(\Delta_{x,i})\otimes\mathscr{M}_0^1(\Delta_{y,i})], \quad i=\mathrm{L},\mathrm{R},\\
\Lambda^h &= \mathscr{M}_{-1}^1(\Delta_{\Gamma_1}).
\end{aligned}$$

The mixed finite element (mortar) method reads as follows: compute $p_i^h\in W_i^h$, $\boldsymbol{u}_i^h\in\boldsymbol{V}_i^h$, $\xi^h\in\Lambda^h$, $i=\mathrm{L},\mathrm{R}$, satisfying

$$\begin{aligned}
&(a_{\mathrm{L}}^{-1}\boldsymbol{u}_{\mathrm{L}}^h,\boldsymbol{v}_{\mathrm{L}})-(p_{\mathrm{L}}^h,\nabla\cdot\boldsymbol{v}_{\mathrm{L}})+\langle\xi^h,\boldsymbol{n}\cdot\boldsymbol{v}_{\mathrm{L}}\rangle_{\Gamma_1}=-\langle g_{\mathrm{L}},\boldsymbol{n}\cdot\boldsymbol{v}_{\mathrm{L}}\rangle_{\Gamma_{\mathrm{L}}},\\
&(\nabla\cdot\boldsymbol{u}_{\mathrm{L}}^h,w_{\mathrm{L}})=(f_{\mathrm{L}},w_{\mathrm{L}}),\\
&(a_{\mathrm{R}}^{-1}\boldsymbol{u}_{\mathrm{R}}^h,\boldsymbol{v}_{\mathrm{R}})-(p_{\mathrm{R}}^h,\nabla\cdot\boldsymbol{v}_{\mathrm{R}})-\langle\xi^h,\boldsymbol{n}\cdot\boldsymbol{v}_{\mathrm{R}}\rangle_{\Gamma_1}=-\langle g_{\mathrm{R}},\boldsymbol{n}\cdot\boldsymbol{v}_{\mathrm{R}}\rangle_{\Gamma_{\mathrm{R}}},\\
&(\nabla\cdot\boldsymbol{u}_{\mathrm{R}}^h,w_{\mathrm{R}})=(f_{\mathrm{R}},w_{\mathrm{R}}),\\
&\langle\boldsymbol{n}\cdot(\boldsymbol{u}_{\mathrm{L}}^h-\boldsymbol{u}_{\mathrm{R}}^h),\nu\rangle_{\Gamma_1}=0,
\end{aligned}\tag{2.6}$$

for all $(w_i,\boldsymbol{v}_i,\nu)\in(W_i^h,\boldsymbol{V}_i^h,\Lambda^h)$, $i=\mathrm{L},\mathrm{R}$. This yields a discrete system of the form

$$\begin{bmatrix}
M_{\mathrm{L}} & -B_{\mathrm{L}} & 0 & 0 & C_{\mathrm{L}}\\
B_{\mathrm{L}}^{\mathrm{T}} & 0 & 0 & 0 & 0\\
0 & 0 & M_{\mathrm{R}} & -B_{\mathrm{R}} & C_{\mathrm{R}}\\
0 & 0 & B_{\mathrm{R}}^{\mathrm{T}} & 0 & 0\\
C_{\mathrm{L}}^{\mathrm{T}} & 0 & C_{\mathrm{R}}^{\mathrm{T}} & 0 & 0
\end{bmatrix}
\begin{bmatrix}
u_{\mathrm{L}}^h\\ p_{\mathrm{L}}^h\\ u_{\mathrm{R}}^h\\ p_{\mathrm{R}}^h\\ \xi^h
\end{bmatrix}
=
\begin{bmatrix}
-D_{\mathrm{L}}\\ F_{\mathrm{L}}\\ -D_{\mathrm{R}}\\ F_{\mathrm{R}}\\ 0
\end{bmatrix},\tag{2.7}$$

where we abuse notation to let u_i^h, p_i^h and ξ^h denote the vector of nodal values for the finite element functions.

2.3 *Geometrically coupled finite volume discretization*

The standard formulation of the finite volume method eschews a variational formulation of the problem, so there is no natural description of a weak imposition of the coupling conditions in that formulation. Moreover, the standard finite volume method provides approximate values of p only at cell centres while

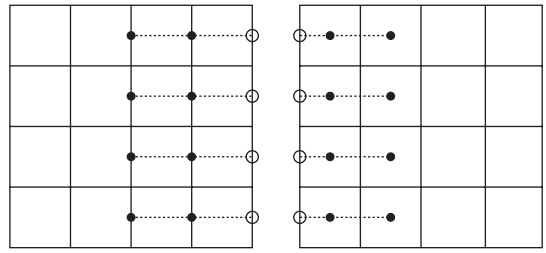

FIG. 3. Extrapolation to the interface. Left: Neumann values on the interface are computed by linear extrapolation of the last two available flux values, which are differences of state values. Right: Dirichlet values on the interface are computed by linear extrapolation of the last two available state values.

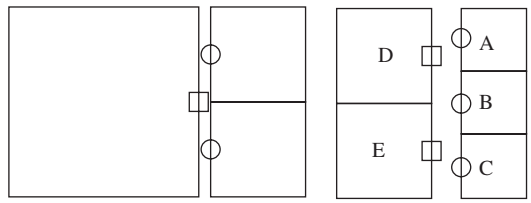

FIG. 4. Averaging or broadcasting of extrapolated values. Left: in the case of constant extrapolation, the last available state or flux value is simply used as the interface value. Right: weighted averaging of state and flux values when cell widths do not share an integer ratio.

approximate values for u along cell boundaries are obtained by differencing the p values. These characteristics motivate the use of 'geometric' coupling techniques that employ a combination of extrapolation and averaging to provide coupling values of both unknowns along the interface. The motivation for this approach is reinforced in the context of iterative solution of the coupled problems, where well-posed problems are created on each subdomain using interface boundary conditions obtained from the other subdomain. In this approach, it is necessary to couple the coarser side using state values extrapolated from the finer side solution, while the finer side must be coupled to flux values, which are themselves differences of state values, extrapolated from the coarser solution. Reversing this arrangement can lead to a singular system.

To obtain values on the interface, we employ either linear or constant extrapolation. We illustrate linear extrapolation in Fig. 3. We compute the extrapolated values by computing a linear or constant interpolant, which is then evaluated at the interface boundary. We denote the extrapolated values using the operators $P_{\mathrm{R}\to\mathrm{L}}(p_{\mathrm{R}}^h)$ and $P_{\mathrm{L}\to\mathrm{R}}(p_{\mathrm{L}}^h)$. When the cells on either side of the interface do not match, then weighted averaging and 'broadcasting' schemes are used to generate values. In Fig. 4, we illustrate the averaging and broadcasting schemes when two cells on the right match one cell on the left. The state values at the two circle locations are averaged and used at the square location. The flux value at the square location is 'broadcast' to both of the circle locations. When the cell widths on the coarse and fine side of the interface do not share an integer ratio, then a suitable averaging of values is used. For example, in the arrangement of 2 cells next to 3 cells pictured in Fig. 4, the state value at location D is set equal to $\frac{2}{3}$ the state value at location A plus $\frac{1}{3}$ the state value at location B. The flux value at location A is set equal to the flux value at location D, while the flux value used at location B is set equal to half the flux value at D plus half the flux value at E.

We formulate the finite volume method as an RT0 mixed finite element method employing a special quadrature formula, following Russell & Wheeler (1983) and Weiser & Wheeler (1988). This provides a foundation for deriving an *a posteriori* error analysis for the finite volume scheme; see Estep *et al.* (2009a). The version of (2.6) equivalent to a finite volume method reads as follows: compute $p_i^h \in W_i^h$, $\boldsymbol{u}_i^h \in \boldsymbol{V}_i^h$, $\xi^h \in \Lambda^h$, $i = \mathrm{L}, \mathrm{R}$, satisfying

$$\begin{aligned}
&(a_{\mathrm{L}}^{-1}\boldsymbol{u}_{\mathrm{L}}^h, \boldsymbol{v}_{\mathrm{L}})_{\mathrm{M,T}} - (p_{\mathrm{L}}^h, \nabla\cdot\boldsymbol{v}_{\mathrm{L}}) + \langle P_{\mathrm{R}\to\mathrm{L}}(p_{\mathrm{R}}^h), \boldsymbol{n}\cdot\boldsymbol{v}_{\mathrm{L}}\rangle_{\Gamma_{\mathrm{I}}} = -\langle g_{\mathrm{L}}, \boldsymbol{n}\cdot\boldsymbol{v}_{\mathrm{L}}\rangle_{\Gamma_{\mathrm{L}},M},\\
&(\nabla\cdot u_{h_L}, w_{\mathrm{L}}) = (f_{\mathrm{L}}, w_{\mathrm{L}}),\\
&(a_{\mathrm{R}}^{-1}\boldsymbol{u}_{\mathrm{R}}^h, \boldsymbol{v}_{\mathrm{R}})_{\mathrm{M,T}} - (p_{\mathrm{R}}^h, \nabla\cdot\boldsymbol{v}_{\mathrm{R}}) - \langle \xi^h, \boldsymbol{n}\cdot\boldsymbol{v}_{\mathrm{R}}\rangle_{\Gamma_{\mathrm{I}}} = -\langle g_{\mathrm{R}}, \boldsymbol{n}\cdot\boldsymbol{v}_{\mathrm{R}}\rangle_{\Gamma_{\mathrm{R}},M},\\
&(\nabla\cdot\boldsymbol{u}_{\mathrm{R}}^h, w_{\mathrm{R}}) = (f_{\mathrm{R}}, w_{\mathrm{R}}),\\
&\langle (P_{\mathrm{L}\to\mathrm{R}}(p_{\mathrm{L}}^h) - \boldsymbol{n}\cdot\boldsymbol{u}_{\mathrm{R}}^h), \nu\rangle_{\Gamma_I} = 0,
\end{aligned} \tag{2.8}$$

for all $(w_i, \boldsymbol{v}_i, \nu) \in (W_i^h, \boldsymbol{V}_i^h, \Lambda^h)$, $i = \mathrm{L}, \mathrm{R}$. Here, we employ the approximate inner product

$$(\boldsymbol{u}^h, \boldsymbol{v})_{\mathrm{M,T}} = (u_x^h, v_x)_{T_x,M_y} + (u_y^h, v_y)_{M_x,T_y},$$

where $M_{(\cdot)}$ and $T_{(\cdot)}$ denote the midpoint and trapezoidal quadrature rules in the x and y directions as indicated, while $\langle\cdot,\cdot\rangle_{\Gamma_i,M}$ denotes the midpoint rule for $i = \mathrm{L}, \mathrm{R}$. Note that the quadrature formulas are applied internally on each cell, so potential discontinuities in a and f across Γ_I cause no difficulty.

This yields a discrete system of the form

$$\begin{bmatrix} M_{\mathrm{L}} & -B_{\mathrm{L}} & 0 & Q_D & 0\\ B_{\mathrm{L}}^{\mathrm{T}} & 0 & 0 & 0 & 0\\ 0 & 0 & M_{\mathrm{R}} & -B_{\mathrm{R}} & C_{\mathrm{R}}\\ 0 & 0 & B_{\mathrm{R}}^{\mathrm{T}} & 0 & 0\\ 0 & Q_N & C_{\mathrm{R}}^{\mathrm{T}} & 0 & 0 \end{bmatrix} \begin{bmatrix} u_{\mathrm{L}}^h\\ p_{\mathrm{L}}^h\\ u_{\mathrm{R}}^h\\ p_{\mathrm{R}}^h\\ \xi^h \end{bmatrix} = \begin{bmatrix} -D_{\mathrm{L}}\\ F_{\mathrm{L}}\\ -D_{\mathrm{R}}\\ F_{\mathrm{R}}\\ 0 \end{bmatrix}, \tag{2.9}$$

which should be compared with (2.7).

It is possible to eliminate the unknowns u_i^h, $i = \mathrm{L}, \mathrm{R}$ and ξ^h, to reduce (2.9) to a system for p_i^h of the form

$$\begin{bmatrix} A_{\mathrm{L}} & C_D\\ C_N & A_{\mathrm{R}} \end{bmatrix} \begin{bmatrix} p_{\mathrm{L}}^h\\ p_{\mathrm{R}}^h \end{bmatrix} = \begin{bmatrix} F_{\mathrm{L}}\\ F_{\mathrm{R}} \end{bmatrix}. \tag{2.10}$$

The averaging and broadcasting are incorporated into the 'coupling Dirichlet' and 'coupling Neumann' matrices C_{D} and C_{N}. This is the same system that is constructed by using a finite volume approach directly.

We have verified through numerical experiments that the p component of the solution of (2.9) is identical to the solution of (2.10). Furthermore, the u component of the solution of (2.9) is identical to the u values obtained by differencing the solution of (2.10) to approximate ∇p at the cell boundaries and evaluating the diffusivity at the cell boundaries. The ξ component of the solution of (2.9) has no counterpart in the solution of (2.10).

3. *A posteriori* error analysis

Our goal is to derive an *a posteriori* error estimate for the quantity of interest

$$(e_{\boldsymbol{u}_\mathrm{L}}, \boldsymbol{\psi}_{\boldsymbol{u}_\mathrm{L}}) + (e_{p_\mathrm{L}}, \psi_{p_\mathrm{L}}) + (e_{\boldsymbol{u}_\mathrm{R}}, \boldsymbol{\psi}_{\boldsymbol{u}_\mathrm{R}}) + (e_{p_\mathrm{R}}, \psi_{p_\mathrm{R}}) + \langle e_\xi, \psi_\xi \rangle_{\Gamma_\mathrm{I}}, \tag{3.1}$$

where $\boldsymbol{\psi}_{\boldsymbol{u}_\mathrm{L}}, \psi_{p_\mathrm{L}}, \boldsymbol{\psi}_{\boldsymbol{u}_\mathrm{R}}, \psi_{p_\mathrm{R}}$ and ψ_ξ are given L^2 functions and $e_{(\cdot)}$ denotes the error in the corresponding variables. We define the generalized Green's function corresponding to these functionals using the adjoint problem

$$\begin{cases} a_\mathrm{L}^{-1}\boldsymbol{\phi}_\mathrm{L} - \nabla\zeta_\mathrm{L} = \boldsymbol{\psi}_{\boldsymbol{u}_\mathrm{L}} & \text{on } \Omega_\mathrm{L}, \\ -\nabla\cdot\boldsymbol{\phi}_\mathrm{L} = \psi_{p_\mathrm{L}} & \text{on } \Omega_\mathrm{L}, \\ \zeta_\mathrm{L} = 0 & \text{on } \Gamma_\mathrm{L}, \end{cases} \tag{3.2}$$

$$\begin{cases} a_\mathrm{R}^{-1}\boldsymbol{\phi}_\mathrm{R} - \nabla\zeta_\mathrm{R} = \boldsymbol{\psi}_{\boldsymbol{u}_\mathrm{R}} & \text{on } \Omega_\mathrm{R}, \\ -\nabla\cdot\boldsymbol{\phi}_\mathrm{R} = \psi_{p_\mathrm{R}} & \text{on } \Omega_\mathrm{R}, \\ \zeta_\mathrm{R} = 0 & \text{on } \Gamma_\mathrm{R}, \end{cases} \tag{3.3}$$

$$\begin{cases} \beta \equiv \zeta_\mathrm{L} = \zeta_\mathrm{R} & \text{on } \Gamma_\mathrm{I}, \\ \boldsymbol{n}\cdot(\boldsymbol{\phi}_\mathrm{L} - \boldsymbol{\phi}_\mathrm{R}) = \psi_\xi & \text{on } \Gamma_\mathrm{I}. \end{cases} \tag{3.4}$$

The *a posteriori* error estimates explicitly depend on $\boldsymbol{\phi}_\mathrm{L}, \zeta_\mathrm{L}, \boldsymbol{\phi}_\mathrm{R}$ and ζ_R.

3.1 *Estimate for mortar mixed finite element method*

We first derive an estimate for the mortar finite element method assuming all integrals in the weak formulation are computed exactly. We begin by substituting (3.2–3.4) for the various ψ's in (3.1) and applying the divergence theorem:

$$\begin{aligned} &(e_{\boldsymbol{u}_\mathrm{L}}, \boldsymbol{\psi}_{\boldsymbol{u}_\mathrm{L}}) + (e_{p_\mathrm{L}}, \psi_{p_\mathrm{L}}) + (e_{\boldsymbol{u}_\mathrm{R}}, \boldsymbol{\psi}_{\boldsymbol{u}_\mathrm{R}}) + (e_{p_\mathrm{R}}, \psi_{p_\mathrm{R}}) + \langle e_\xi, \psi_\xi \rangle_{\Gamma_\mathrm{I}} \\ &\quad = (e_{\boldsymbol{u}_\mathrm{L}}, a_\mathrm{L}^{-1}\boldsymbol{\phi}_\mathrm{L}) + (\nabla\cdot e_{\boldsymbol{u}_\mathrm{L}}, \zeta_\mathrm{L}) - \langle \boldsymbol{n}\cdot e_{\boldsymbol{u}_\mathrm{L}}, \beta\rangle_{\Gamma_\mathrm{I}} - (e_{p_\mathrm{L}}, \nabla\cdot\boldsymbol{\phi}_\mathrm{L}) \\ &\qquad + (e_{\boldsymbol{u}_\mathrm{R}}, a_\mathrm{R}^{-1}\boldsymbol{\phi}_\mathrm{R}) + (\nabla\cdot e_{\boldsymbol{u}_\mathrm{R}}, \zeta_\mathrm{R}) + \langle \boldsymbol{n}\cdot e_{\boldsymbol{u}_\mathrm{R}}, \beta\rangle_{\Gamma_\mathrm{I}} - (e_{p_\mathrm{R}}, \nabla\cdot\boldsymbol{\phi}_\mathrm{R}) + \langle e_\xi, \boldsymbol{n}\cdot(\boldsymbol{\phi}_\mathrm{L} - \boldsymbol{\phi}_\mathrm{R})\rangle_{\Gamma_\mathrm{I}}. \end{aligned} \tag{3.5}$$

Expanding on the right and subtracting

$$\begin{aligned} &(a_\mathrm{L}^{-1}\boldsymbol{u}_\mathrm{L}, \boldsymbol{\phi}_\mathrm{L}) - (p_\mathrm{L}, \nabla\cdot\boldsymbol{\phi}_\mathrm{L}) + \langle \xi, \boldsymbol{n}\cdot\boldsymbol{\phi}_\mathrm{L}\rangle_{\Gamma_\mathrm{I}} + \langle g_\mathrm{L}, \boldsymbol{n}\cdot\boldsymbol{\phi}_\mathrm{L}\rangle_{\Gamma_\mathrm{L}} \\ &\quad + (\nabla\cdot\boldsymbol{u}_\mathrm{L}, \zeta_\mathrm{L}) - (f_\mathrm{L}, \zeta_\mathrm{L}) + (a_\mathrm{R}^{-1}\boldsymbol{u}_\mathrm{R}, \boldsymbol{\phi}_\mathrm{R}) - (p_\mathrm{R}, \nabla\cdot\boldsymbol{\phi}_\mathrm{R}) - \langle \xi, \boldsymbol{n}\cdot\boldsymbol{\phi}_\mathrm{R}\rangle_{\Gamma_\mathrm{I}} + \langle g_\mathrm{R}, \boldsymbol{n}\cdot\boldsymbol{\phi}_\mathrm{R}\rangle_{\Gamma_\mathrm{R}} \\ &\quad + (\nabla\cdot\boldsymbol{u}_\mathrm{R}, \zeta_\mathrm{R}) - (f_\mathrm{R}, \zeta_\mathrm{R}) - \langle \boldsymbol{n}\cdot(\boldsymbol{u}_\mathrm{L} - \boldsymbol{u}_\mathrm{R}), \beta\rangle_{\Gamma_\mathrm{I}} = 0, \end{aligned}$$

obtained by substituting the adjoint solution as test functions into the forward weak form (2.5), gives

$$\begin{aligned}
&(e_{\boldsymbol{u}_{\mathrm{L}}}, \boldsymbol{\psi}_{\boldsymbol{u}_{\mathrm{L}}}) + (e_{p_{\mathrm{L}}}, \psi_{p_{\mathrm{L}}}) + (e_{\boldsymbol{u}_{\mathrm{R}}}, \boldsymbol{\psi}_{\boldsymbol{u}_{\mathrm{R}}}) + (e_{p_{\mathrm{R}}}, \psi_{p_{\mathrm{R}}}) + \langle e_\xi, \psi_\xi \rangle_{\Gamma_{\mathrm{I}}} \\
&\quad = -(a_{\mathrm{L}}^{-1}\boldsymbol{u}_{\mathrm{L}}^h, \boldsymbol{\phi}_{\mathrm{L}}) + (p_{\mathrm{L}}^h, \nabla\cdot\boldsymbol{\phi}_{\mathrm{L}}) - \langle g_{\mathrm{L}}, \boldsymbol{n}\cdot\boldsymbol{\phi}_{\mathrm{L}}\rangle_{\Gamma_{\mathrm{L}}} - \langle \xi^h, \boldsymbol{n}\cdot\boldsymbol{\phi}_{\mathrm{L}}\rangle_{\Gamma_{\mathrm{I}}} + (f_{\mathrm{L}}, \zeta_{\mathrm{L}}) - (\nabla\cdot\boldsymbol{u}_{\mathrm{L}}^h, \zeta_{\mathrm{L}}) \\
&\qquad - (a_{\mathrm{R}}^{-1}\boldsymbol{u}_{\mathrm{R}}^h, \boldsymbol{\phi}_{\mathrm{R}}) + (p_{\mathrm{R}}^h, \nabla\cdot\boldsymbol{\phi}_{\mathrm{R}}) - \langle g_{\mathrm{R}}, \boldsymbol{n}\cdot\boldsymbol{\phi}_{\mathrm{R}}\rangle_{\Gamma_{\mathrm{R}}} + \langle \xi^h, \boldsymbol{n}\cdot\boldsymbol{\phi}_{\mathrm{R}}\rangle_{\Gamma_{\mathrm{I}}} \\
&\qquad + (f_{\mathrm{R}}, \zeta_{\mathrm{R}}) - (\nabla\cdot\boldsymbol{u}_{\mathrm{R}}^h, \zeta_{\mathrm{R}}) + \langle \boldsymbol{n}\cdot(\boldsymbol{u}_{\mathrm{L}}^h - \boldsymbol{u}_{\mathrm{R}}^h), \beta\rangle_{\Gamma_{\mathrm{I}}}.
\end{aligned} \tag{3.6}$$

We rewrite this as

$$\begin{aligned}
&(e_{\boldsymbol{u}_{\mathrm{L}}}, \boldsymbol{\psi}_{\boldsymbol{u}_{\mathrm{L}}}) + (e_{p_{\mathrm{L}}}, \psi_{p_{\mathrm{L}}}) + (e_{\boldsymbol{u}_{\mathrm{R}}}, \boldsymbol{\psi}_{\boldsymbol{u}_{\mathrm{R}}}) + (e_{p_{\mathrm{R}}}, \psi_{p_{\mathrm{R}}}) + \langle e_\xi, \psi_\xi \rangle_{\Gamma_{\mathrm{I}}} \\
&\quad = (\boldsymbol{R}_{\boldsymbol{u}_{\mathrm{L}}}, \boldsymbol{\phi}_{\mathrm{L}}) + (R_{p_{\mathrm{L}}}, \zeta_{\mathrm{L}}) + (\boldsymbol{R}_{\boldsymbol{u}_{\mathrm{R}}}, \boldsymbol{\phi}_{\mathrm{R}}) + (R_{p_{\mathrm{R}}}, \zeta_{\mathrm{R}}) + \langle R_\xi, \beta\rangle_{\Gamma_{\mathrm{I}}},
\end{aligned} \tag{3.7}$$

wherein the residuals are given by

$$\begin{aligned}
&\boldsymbol{R}_{\boldsymbol{u}_{\mathrm{L}}} = -a_{\mathrm{L}}^{-1}\boldsymbol{u}_{\mathrm{L}}^h - \nabla p_{\mathrm{L}}^h, \quad \boldsymbol{R}_{\boldsymbol{u}_{\mathrm{R}}} = -a_{\mathrm{R}}^{-1}\boldsymbol{u}_{\mathrm{R}}^h - \nabla p_{\mathrm{R}}^h, \\
&R_{p_{\mathrm{L}}} = f_{\mathrm{L}} - \nabla\cdot\boldsymbol{u}_{\mathrm{L}}^h, \quad R_{p_{\mathrm{R}}} = f_{\mathrm{R}} - \nabla\cdot\boldsymbol{u}_{\mathrm{R}}^h, \quad R_\xi = \boldsymbol{n}\cdot(\boldsymbol{u}_{\mathrm{L}}^h - \boldsymbol{u}_{\mathrm{R}}^h).
\end{aligned}$$

Note that the divergence theorem implies

$$\begin{aligned}
(\boldsymbol{R}_{\boldsymbol{u}_{\mathrm{L}}}, \boldsymbol{\phi}_{\mathrm{L}}) &= -(a_{\mathrm{L}}^{-1}\boldsymbol{u}_{\mathrm{L}}^h, \boldsymbol{\phi}_{\mathrm{L}}) + (p_{\mathrm{L}}^h, \nabla\cdot\boldsymbol{\phi}_{\mathrm{L}}) - \langle p_{\mathrm{L}}^h, \boldsymbol{n}\cdot\boldsymbol{\phi}_{\mathrm{L}}\rangle_{\partial\Omega_{\mathrm{L}}} \\
&= -(a_{\mathrm{L}}^{-1}\boldsymbol{u}_{h_{\mathrm{L}}}, \boldsymbol{\phi}_{\mathrm{L}}) + (p_{\mathrm{L}}^h, \nabla\cdot\boldsymbol{\phi}_{\mathrm{L}}) - \langle g_{\mathrm{L}}, \boldsymbol{n}\cdot\boldsymbol{\phi}_{\mathrm{L}}\rangle_{\Gamma_{\mathrm{L}}} - \langle \xi^h, \boldsymbol{n}\cdot\boldsymbol{\phi}_{\mathrm{L}}\rangle_{\Gamma_{\mathrm{I}}}.
\end{aligned}$$

Also note that $\beta = \zeta_{\mathrm{L}} = \zeta_{\mathrm{R}}$ for the continuous adjoint solution, but β is distinct from ζ_{L} and ζ_{R} for the discrete solution.

Next, we use Galerkin orthogonality. We introduce projection operators that map into the finite element space of the discrete forward solution:

$$\begin{aligned}
&P_{\mathrm{L}}^h : L^2(\Omega_{\mathrm{L}}) \to W_{\mathrm{L}}^h, \quad P_{\mathrm{R}}^h : L^2(\Omega_{\mathrm{R}}) \to W_{\mathrm{R}}^h, \\
&\Pi_{\mathrm{L}}^h : L^2(\Omega_{\mathrm{L}}) \to \boldsymbol{V}_{\mathrm{L}}^h, \quad \Pi_{\mathrm{R}}^h : L^2(\Omega_{\mathrm{R}}) \to \boldsymbol{V}_{\mathrm{R}}^h, \quad Z^h : L^2(\Gamma_{\mathrm{I}}) \to \Lambda^h.
\end{aligned}$$

The actual choice of projection is immaterial for the estimate. In practice, we employ a combination of restriction and averaging. Without quadrature, Galerkin orthogonality for (2.6) is expressed as

$$(\boldsymbol{R}_{\boldsymbol{u}_{\mathrm{L}}}, \Pi_{\mathrm{L}}^h\boldsymbol{\phi}_{\mathrm{L}}) + (R_{p_{\mathrm{L}}}, P_{\mathrm{L}}^h\zeta_{\mathrm{L}}) + (\boldsymbol{R}_{\boldsymbol{u}_{\mathrm{R}}}, \Pi_{\mathrm{R}}^h\boldsymbol{\phi}_{\mathrm{R}}) + (R_{p_{\mathrm{R}}}, P_{\mathrm{R}}^h\zeta_{\mathrm{R}}) + \langle R_\xi, Z_h\beta\rangle_{\Gamma_I} = 0,$$

and subtracting gives the following result.

THEOREM 3.1 The errors for the mixed finite element method (2.6) without quadrature satisfy

$$\begin{aligned}
&(e_{p_{\mathrm{L}}}, \psi_{p_{\mathrm{L}}}) + (e_{\boldsymbol{u}_{\mathrm{L}}}, \boldsymbol{\psi}_{\boldsymbol{u}_{\mathrm{L}}}) + (e_{p_{\mathrm{R}}}, \psi_{p_{\mathrm{R}}}) + (e_{\boldsymbol{u}_{\mathrm{R}}}, \boldsymbol{\psi}_{\boldsymbol{u}_{\mathrm{R}}}) + \langle e_\xi, \psi_\xi \rangle_{\Gamma_{\mathrm{I}}} \\
&\quad = (\boldsymbol{R}_{\boldsymbol{u}_{\mathrm{L}}}, \boldsymbol{\phi}_{\mathrm{L}} - \Pi_{\mathrm{L}}^h\boldsymbol{\phi}_{\mathrm{L}}) + (R_{p_{\mathrm{L}}}, \zeta_{\mathrm{L}} - P_{\mathrm{L}}^h\zeta_{\mathrm{L}}) \\
&\qquad + (\boldsymbol{R}_{\boldsymbol{u}_{\mathrm{R}}}, \boldsymbol{\phi}_{\mathrm{R}} - \Pi_{\mathrm{R}}^h\boldsymbol{\phi}_{\mathrm{R}}) + (R_{p_{\mathrm{R}}}, \zeta_{\mathrm{R}} - P_{\mathrm{R}}^h\zeta_{\mathrm{R}}) + \langle R_\xi, \beta - Z_h\beta\rangle_{\Gamma_{\mathrm{I}}},
\end{aligned} \tag{3.8}$$

wherein the quantities on the right-hand side are computable provided the true adjoint solution is available.

In practice, we employ a numerical solution of the adjoint problem. To emphasize this, we state the following corollary that involves numerical adjoint quantities.

COROLLARY 3.2 Provided that the projection operators P_{L}^h, P_{R}^h, Π_{L}^h, Π_{R}^h and Z_h are bounded in L^2, the errors for the mixed finite element method (2.6) without quadrature can be estimated as

$$\begin{aligned}(e_{p_{\mathrm{L}}}, \psi_{p_{\mathrm{L}}}) + (e_{\boldsymbol{u}_{\mathrm{L}}}, \boldsymbol{\psi}_{\boldsymbol{u}_{\mathrm{L}}}) + (e_{p_{\mathrm{R}}}, \psi_{p_{\mathrm{R}}}) + (e_{\boldsymbol{u}_{\mathrm{R}}}, \boldsymbol{\psi}_{\boldsymbol{u}_{\mathrm{R}}}) + \langle e_\xi, \psi_\xi \rangle_{\Gamma_{\mathrm{I}}} \\ \approx (\boldsymbol{R}_{\boldsymbol{u}_{\mathrm{L}}}, \boldsymbol{\phi}_{\mathrm{L}}^h - \Pi_{\mathrm{L}}^h \boldsymbol{\phi}_{\mathrm{L}}^h) + (R_{p_{\mathrm{L}}}, \zeta_{\mathrm{L}}^h - P_{\mathrm{L}}^h \zeta_{\mathrm{L}}^h) \\ + (\boldsymbol{R}_{\boldsymbol{u}_{\mathrm{R}}}, \boldsymbol{\phi}_{\mathrm{R}}^h - \Pi_{\mathrm{R}}^h \boldsymbol{\phi}_{\mathrm{R}}^h) + (R_{p_{\mathrm{R}}}, \zeta_{\mathrm{R}}^h - P_{\mathrm{R}}^h \zeta_{\mathrm{R}}^h) + \langle R_\xi, \beta^h - Z_h \beta^h \rangle_{\Gamma_{\mathrm{I}}},\end{aligned} \tag{3.9}$$

for numerical solutions $\boldsymbol{\phi}_{\mathrm{L}} \approx \boldsymbol{\phi}_{\mathrm{L}}^h$, $\zeta_{\mathrm{L}} \approx \zeta_{\mathrm{L}}^h$, $\boldsymbol{\phi}_{\mathrm{R}} \approx \boldsymbol{\phi}_{\mathrm{R}}^h$, $\zeta_{\mathrm{R}} \approx \zeta_{\mathrm{R}}^h$ and $\beta \approx \beta^h$. In this approximation, the errors are to be measured in the L^2 norm.

The proof follows from the triangle inequality and the definition of the operator norm. That is, the absolute value of the difference between the right-hand sides of (3.8) and (3.9) is bounded by

$$\begin{aligned}(1 + \|\Pi_{\mathrm{L}}^h\|)\|\boldsymbol{R}_{\boldsymbol{u}_{\mathrm{L}}}\|_2 \|\boldsymbol{\phi}_{\mathrm{L}} - \boldsymbol{\phi}_{\mathrm{L}}^h\|_2 + (1 + \|P_{\mathrm{L}}^h\|)\|R_{p_{\mathrm{L}}}\|_2 \|\zeta_{\mathrm{L}} - \zeta_{\mathrm{L}}^h\|_2 \\ + (1 + \|\Pi_{\mathrm{R}}^h\|)\|\boldsymbol{R}_{\boldsymbol{u}_{\mathrm{R}}}\|_2 \|\boldsymbol{\phi}_{\mathrm{R}} - \boldsymbol{\phi}_{\mathrm{R}}^h\|_2 + (1 + \|P_{\mathrm{R}}^h\|)\|R_{p_{\mathrm{R}}}\|_2 \|\zeta_{\mathrm{R}} - \zeta_{\mathrm{R}}^h\|_2 \\ + (1 + \|Z_h\|)\|R_\xi\|_{2,\Gamma_{\mathrm{I}}} \|\beta - \beta^h\|_{2,\Gamma_{\mathrm{I}}}.\end{aligned}$$

In order to obtain accurate estimates, the numerical adjoint solutions must be sufficiently accurate. Generally, this is satisfied by solving the adjoint problems either using a higher-order numerical method or using a mesh sufficiently refined from the one used for the forward discretization. In the context of finite volume discretizations, the second approach is generally easier to implement. In our numerical examples we use a finer grid and the accuracy of this approach is illustrated in Section 4.1.

3.2 *Estimate for finite volume methods using geometric coupling*

3.2.1 *The effect of quadrature.* We first derive an estimate for the mixed finite element method (2.6) with quadrature, which can be applied, say, if f_i, g_i and a_i are continuous in Ω_i, $i = \mathrm{L}, \mathrm{R}$. With quadrature, Galerkin orthogonality is expressed as

$$(\boldsymbol{R}_{\boldsymbol{u}_{\mathrm{L}}}, \Pi_{\mathrm{L}}^h \boldsymbol{\phi}_{\mathrm{L}})_{\mathrm{Q}} + (R_{p_{\mathrm{L}}}, P_{\mathrm{L}}^h \zeta_{\mathrm{L}})_{\mathrm{Q}} + (\boldsymbol{R}_{\boldsymbol{u}_{\mathrm{R}}}, \Pi_{\mathrm{R}}^h \boldsymbol{\phi}_{\mathrm{R}})_{\mathrm{Q}} + (R_{p_{\mathrm{R}}}, P_{\mathrm{R}}^h \zeta_{\mathrm{R}})_{\mathrm{Q}} + \langle R_\xi, Z_h \beta \rangle_{\mathrm{Q},\Gamma_I} = 0,$$

where we use the subscript Q to denote the approximate inner product using quadrature. It is important to distinguish residuals associated with approximating the solution spaces using finite-dimensional polynomial spaces from residuals associated with approximating the integrals defining the variational formulation. We rewrite Galerkin orthogonality as

$$\begin{aligned}(\boldsymbol{R}_{\boldsymbol{u}_{\mathrm{L}}}, \Pi_{\mathrm{L}}^h \boldsymbol{\phi}_{\mathrm{L}}) + (R_{p_{\mathrm{L}}}, P_{\mathrm{L}}^h \zeta_{\mathrm{L}}) + (\boldsymbol{R}_{\boldsymbol{u}_{\mathrm{R}}}, \Pi_{\mathrm{R}}^h \boldsymbol{\phi}_{\mathrm{R}}) + (R_{p_{\mathrm{R}}}, P_{\mathrm{R}}^h \zeta_{\mathrm{R}}) + \langle R_\xi, Z_h \beta \rangle_{\Gamma_{\mathrm{I}}} \\ - \mathrm{QE}_{\boldsymbol{u}_{\mathrm{L}}}(\Pi_{\mathrm{L}}^h \boldsymbol{\phi}_{\mathrm{L}}) - \mathrm{QE}_{p_{\mathrm{L}}}(P_{\mathrm{L}}^h \zeta_{\mathrm{L}}) - \mathrm{QE}_{\boldsymbol{u}_{\mathrm{R}}}(\Pi_{\mathrm{R}}^h \boldsymbol{\phi}_{\mathrm{R}}) - \mathrm{QE}_{p_{\mathrm{R}}}(P_{\mathrm{R}}^h \zeta_{\mathrm{R}}) - \mathrm{QE}_\xi(Z^h \beta) = 0,\end{aligned}$$

with

$$\begin{aligned}
\mathrm{QE}_{\boldsymbol{u}_\mathrm{L}}(\Pi_\mathrm{L}^h\boldsymbol{\phi}_\mathrm{L}) &= (\boldsymbol{R}_{\boldsymbol{u}_\mathrm{L}}, \Pi_\mathrm{L}^h\boldsymbol{\phi}_\mathrm{L}) - (\boldsymbol{R}_{\boldsymbol{u}_\mathrm{L}}, \Pi_\mathrm{L}^h\boldsymbol{\phi}_\mathrm{L})_\mathrm{Q},\\
\mathrm{QE}_{p_\mathrm{L}}(P_\mathrm{L}^h\zeta_\mathrm{L}) &= (R_{p_\mathrm{L}}, P_\mathrm{L}^h\zeta_\mathrm{L}) - (R_{p_\mathrm{L}}, P_\mathrm{L}^h\zeta_\mathrm{L})_\mathrm{Q},\\
\mathrm{QE}_{\boldsymbol{u}_\mathrm{R}}(\Pi_\mathrm{R}^h\boldsymbol{\phi}_\mathrm{R}) &= (\boldsymbol{R}_{\boldsymbol{u}_\mathrm{R}}, \Pi_\mathrm{R}^h\boldsymbol{\phi}_\mathrm{R}) - (\boldsymbol{R}_{\boldsymbol{u}_\mathrm{R}}, \Pi_\mathrm{R}^h\boldsymbol{\phi}_\mathrm{R})_\mathrm{Q},\\
\mathrm{QE}_{p_\mathrm{R}}(P_\mathrm{R}^h\zeta_\mathrm{R}) &= (R_{p_\mathrm{R}}, P_\mathrm{R}^h\zeta_\mathrm{R}) - (R_{p_\mathrm{R}}, P_\mathrm{R}^h\zeta_\mathrm{R})_\mathrm{Q},\\
\mathrm{QE}_{\xi}(Z^h\beta) &= \langle R_\xi, Z_h\beta\rangle_{\Gamma_\mathrm{I}} - \langle R_\xi, Z_h\beta\rangle_{\mathrm{Q},\Gamma_I}.
\end{aligned}$$

This gives the following *a posteriori* estimate for the mixed finite element method with quadrature.

THEOREM 3.3 If f_i, g_i and a_i are continuous in Ω_i, $i = \mathrm{L}, \mathrm{R}$, then the errors for the mixed finite element method (2.6) with quadrature satisfy

$$\begin{aligned}
&(e_{p_\mathrm{L}}, \psi_{p_\mathrm{L}}) + (e_{\boldsymbol{u}_\mathrm{L}}, \boldsymbol{\psi}_{\boldsymbol{u}_\mathrm{L}}) + (e_{p_\mathrm{R}}, \psi_{p_\mathrm{R}}) + (e_{\boldsymbol{u}_\mathrm{R}}, \boldsymbol{\psi}_{\boldsymbol{u}_\mathrm{R}}) + \langle e_\xi, \psi_\xi\rangle_{\Gamma_\mathrm{I}}\\
&\quad= (\boldsymbol{R}_{\boldsymbol{u}_\mathrm{L}}, \boldsymbol{\phi}_\mathrm{L} - \Pi_\mathrm{L}^h\boldsymbol{\phi}_\mathrm{L}) + (R_{p_\mathrm{L}}, \zeta_\mathrm{L} - P_\mathrm{L}^h\zeta_\mathrm{L})\\
&\qquad+ (\boldsymbol{R}_{\boldsymbol{u}_\mathrm{R}}, \boldsymbol{\phi}_\mathrm{R} - \Pi_\mathrm{R}^h\boldsymbol{\phi}_\mathrm{R}) + (R_{p_\mathrm{R}}, \zeta_\mathrm{R} - P_\mathrm{R}^h\zeta_\mathrm{R}) + \langle R_\xi, \beta - Z_h\beta\rangle_{\Gamma_\mathrm{I}}\\
&\qquad+ \mathrm{QE}_{\boldsymbol{u}_\mathrm{L}}(\Pi_\mathrm{L}^h\boldsymbol{\phi}_\mathrm{L}) + \mathrm{QE}_{p_\mathrm{L}}(P_\mathrm{L}^h\zeta_\mathrm{L}) + \mathrm{QE}_{\boldsymbol{u}_\mathrm{R}}(\Pi_\mathrm{R}^h\boldsymbol{\phi}_\mathrm{R}) + \mathrm{QE}_{p_\mathrm{R}}(P_\mathrm{R}^h\zeta_\mathrm{R}) + \mathrm{QE}_{\xi}(Z^h\beta). \qquad (3.10)
\end{aligned}$$

Note that in the case of using the RT0 finite element space and the midpoint/trapezoidal quadrature rules discussed above, the mixed finite element method reduces to the finite volume method (Russell & Wheeler, 1983; Weiser & Wheeler, 1988; Estep *et al.*, 2009a) and some of the quadrature error terms are zero. These terms are included for generality, so that (3.10) is valid for other combinations of finite element spaces and quadrature.

Note that, in practice, we implement the obvious analogue of Corollary 3.2, which now requires sufficient smoothness of the solution to obtain sufficiently accurate quadrature approximations.

3.2.2 *The effect of geometric coupling.* For the geometric coupling (2.8), Galerkin orthogonality becomes

$$\begin{aligned}
&(\boldsymbol{R}_{\boldsymbol{u}_\mathrm{L}}, \Pi_\mathrm{L}^h\boldsymbol{\phi}_\mathrm{L})_\mathrm{Q} - \langle P_{\mathrm{R}\to\mathrm{L}}(p_\mathrm{R}^h) - \xi^h, \boldsymbol{n}\cdot\Pi_\mathrm{L}^h\boldsymbol{\phi}_\mathrm{L}\rangle_{\mathcal{Q},\Gamma_I} + (R_{p_\mathrm{L}}, P_\mathrm{L}^h\zeta_\mathrm{L})_\mathrm{Q}\\
&\quad+ (\boldsymbol{R}_{\boldsymbol{u}_\mathrm{R}}, \Pi_\mathrm{R}^h\boldsymbol{\phi}_\mathrm{R})_\mathrm{Q} + (R_{p_\mathrm{R}}, P_\mathrm{R}^h\zeta_\mathrm{R})_\mathrm{Q} + \langle R_\xi, Z_h\beta\rangle_{\mathcal{Q},\Gamma_I} - \langle \boldsymbol{n}\cdot\boldsymbol{u}_\mathrm{L}^h - P_{\mathrm{L}\to\mathrm{R}}(p_\mathrm{L}^h), Z^h\beta\rangle_{\mathcal{Q},\Gamma_I} = 0.
\end{aligned}$$

Defining

$$\begin{aligned}
\mathcal{QE}_{\boldsymbol{u}_\mathrm{L}}(\Pi_\mathrm{L}^h\boldsymbol{\phi}_\mathrm{L}) &= (\boldsymbol{R}_{\boldsymbol{u}_\mathrm{L}}, \Pi_\mathrm{L}^h\boldsymbol{\phi}_\mathrm{L}) - (\boldsymbol{R}_{\boldsymbol{u}_\mathrm{L}}, \Pi_\mathrm{L}^h\boldsymbol{\phi}_\mathrm{L})_\mathrm{Q}\\
&\quad+ \langle P_{\mathrm{R}\to\mathrm{L}}(p_\mathrm{R}^h) - \xi^h, \Pi_\mathrm{L}^h\boldsymbol{\phi}_\mathrm{L}\rangle_{\mathcal{Q},\Gamma_I} - \langle P_{\mathrm{R}\to\mathrm{L}}(p_\mathrm{R}^h) - \xi^h, \boldsymbol{n}\cdot\Pi_\mathrm{L}^h\boldsymbol{\phi}_\mathrm{L}\rangle_{\Gamma_\mathrm{I}},\\
\mathcal{QE}_{\xi}(Z^h\phi_1) &= \langle R_\xi, Z_h\beta\rangle_{\Gamma_\mathrm{I}} - \langle R_\xi, Z_h\beta\rangle_{\mathcal{Q},\Gamma_I}\\
&\quad+ \langle \boldsymbol{n}_\mathrm{L}\cdot\boldsymbol{u}_\mathrm{L}^h - P_{\mathrm{L}\to\mathrm{R}}(p_\mathrm{L}^h), Z^h\beta\rangle_{\mathcal{Q},\Gamma_I} - \langle \boldsymbol{n}\cdot\boldsymbol{u}_\mathrm{L}^h - P_{\mathrm{L}\to\mathrm{R}}(p_\mathrm{L}^h), Z^h\beta\rangle_{\Gamma_\mathrm{I}},
\end{aligned}$$

and arguing as above gives the following result.

THEOREM 3.4 If f_i, g_i and a_i are continuous in Ω_i, $i = \mathrm{L}, \mathrm{R}$, then the error for the mixed geometric finite volume method (2.8) satisfies

$$\begin{aligned}
&(e_{p_\mathrm{L}}, \psi_{p_\mathrm{L}}) + (e_{\boldsymbol{u}_\mathrm{L}}, \boldsymbol{\psi}_{\boldsymbol{u}_\mathrm{L}}) + (e_{p_\mathrm{R}}, \psi_{p_\mathrm{R}}) + (e_{\boldsymbol{u}_\mathrm{R}}, \boldsymbol{\psi}_{\boldsymbol{u}_\mathrm{R}}) + \langle e_\xi, \psi_\xi \rangle_{\Gamma_\mathrm{I}} \\
&\quad = (\boldsymbol{R}_{\boldsymbol{u}_\mathrm{L}}, \boldsymbol{\phi}_\mathrm{L} - \Pi^h_\mathrm{L} \boldsymbol{\phi}_\mathrm{L}) + \langle P_{\mathrm{R}\to\mathrm{L}}(p^h_\mathrm{R}) - \xi^h, \boldsymbol{n} \cdot \Pi^h_\mathrm{L} \boldsymbol{\phi}_\mathrm{L} \rangle_{\Gamma_\mathrm{I}} + (R_{p_\mathrm{L}}, \zeta_\mathrm{L} - P^h_\mathrm{L} \zeta_\mathrm{L}) \\
&\qquad + (\boldsymbol{R}_{\boldsymbol{u}_\mathrm{R}}, \boldsymbol{\phi}_\mathrm{R} - \Pi^h_\mathrm{R} \boldsymbol{\phi}_\mathrm{R}) + (R_{p_\mathrm{R}}, \zeta_\mathrm{R} - P^h_\mathrm{R} \zeta_\mathrm{R}) \\
&\qquad + \langle R_\xi, \beta - Z_h \beta \rangle_{\Gamma_\mathrm{I}} + \langle \boldsymbol{n} \cdot \boldsymbol{u}^h_\mathrm{L} - P_{\mathrm{L}\to\mathrm{R}}(p^h_\mathrm{L}), Z^h \beta \rangle_{\Gamma_\mathrm{I}} \\
&\qquad + \mathscr{Q}\mathscr{E}_{\boldsymbol{u}_\mathrm{L}}(\Pi^h_\mathrm{L} \boldsymbol{\phi}_\mathrm{L}) + \mathrm{QE}_{p_\mathrm{L}}(P^h_\mathrm{L} \zeta_\mathrm{L}) + \mathrm{QE}_{\boldsymbol{u}_\mathrm{R}}(\Pi^h_\mathrm{R} \boldsymbol{\phi}_\mathrm{R}) + \mathrm{QE}_{p_\mathrm{R}}(P^h_\mathrm{R} \zeta_\mathrm{R}) + \mathscr{Q}\mathscr{E}_\xi(Z^h \beta). \qquad (3.11)
\end{aligned}$$

Note that, in practice, we implement the obvious analogue of Corollary 3.2, assuming again sufficient smoothness of the solution to obtain sufficiently accurate quadrature approximations.

4. Numerical investigations

In this section, we use the *a posteriori* error estimates to investigate in detail the accuracy of the two approaches to coupling. For all of the investigations, the coarser subdomain Ω_L is given by $x \in [-1, 1]$ and $y \in [-2, 0]$, the finer subdomain Ω_R is given by $x \in [-1, 1]$ and $y \in [0, 2]$ (see Fig. 1) and the interface Γ_I is located along $y = 0$. (Note that here the bottom subdomain is considered as being 'left' and the top one is 'right', in conformance with our convention as to the finer subdomain.) The grids are reported as $n_\mathrm{L} \times m_\mathrm{L}$ for the left domain and $n_\mathrm{R} \times m_\mathrm{R}$ for the right domain, where $n_{(\cdot)}$ corresponds to the number of cells in the x direction (which is also the number of cells along the interface) and $m_{(\cdot)}$ corresponds to the number of cells in the y direction. The boundary conditions for all tests are Dirichlet. To avoid issues arising from iterative solution of the discrete system, we employ direct methods to find the approximate solution to within machine precision.

The quantity of interest is specified by giving the adjoint problem data ψ_{u_x}, ψ_{u_y}, ψ_p and ψ_ξ. The adjoint problem is solved using the same RT0 mixed finite element method, but on a grid that is significantly finer than that of the forward problem, so that the discretization error associated with the adjoint solution has no significant effect on the results.

The functions chosen for the source, diffusivity and adjoint data are either constants or Gaussian functions of the form

$$\frac{a e^{-(y-b)^2}}{\sqrt{2c^2}} + K,$$

which gives a localized 'ridge' centred at $y = b$. In the case of the adjoint data, the Gaussian or constant function being used is normalized so that the area under ψ is equal to 1. The parameter K is nonzero only in the case of diffusivity, where this constant is added to the Gaussian to prevent the diffusivity from approaching zero anywhere in the domain.

In the tests, we report values for the terms in (3.10) and (3.11) that are nonzero. For both the mixed finite element and geometric finite volume methods the following five terms are included:

$$\begin{aligned}
&\mathrm{MFE}_1 \quad \text{or} \quad \mathrm{GFV}_1 = (\boldsymbol{R}_{\boldsymbol{u}_\mathrm{L}}, \boldsymbol{\phi}^h_\mathrm{L} - \Pi^h_\mathrm{L} \boldsymbol{\phi}^h_\mathrm{L}), \\
&\mathrm{MFE}_2 \quad \text{or} \quad \mathrm{GFV}_2 = (\boldsymbol{R}_{\boldsymbol{u}_\mathrm{R}}, \boldsymbol{\phi}^h_\mathrm{R} - \Pi^h_\mathrm{R} \boldsymbol{\phi}^h_\mathrm{R}),
\end{aligned}$$

$$\begin{aligned}
&\text{MFE}_3 \quad \text{or} \quad \text{GFV}_3 = (R_{p_\text{L}}, \zeta_\text{L}^h - P_\text{L}^h \zeta_\text{L}^h),\\
&\text{MFE}_4 \quad \text{or} \quad \text{GFV}_4 = (R_{p_\text{R}}, \zeta_\text{R}^h - P_\text{R}^h \zeta_\text{R}^h),\\
&\text{MFE}_5 \quad \text{or} \quad \text{GFV}_5 = \langle R_\xi, \beta^h - Z_h \beta^h \rangle_{\Gamma_\text{I}}.
\end{aligned}$$

In the geometric finite volume case, we add two additional terms relating to the geometric projections and two additional quadrature terms:

$$\begin{aligned}
\text{GFV}_6 &= \langle P_{\text{R}\to\text{L}}(p_\text{R}^h) - \xi^h, \boldsymbol{n} \cdot \Pi_\text{L}^h \boldsymbol{\phi}_\text{L}^h \rangle_{\Gamma_\text{I}},\\
\text{GFV}_7 &= \langle \boldsymbol{n} \cdot \boldsymbol{u}_\text{L}^h - P_{\text{L}\to\text{R}}(p_\text{L}^h), Z^h \beta^h \rangle_{\Gamma_\text{I}},\\
\text{GFV}_8 &= \mathscr{QE}_{\boldsymbol{u}_\text{L}}(\Pi_\text{L}^h \boldsymbol{\phi}_\text{L}^h),\\
\text{GFV}_9 &= \text{QE}_{\boldsymbol{u}_\text{R}}(\Pi_\text{R}^h \boldsymbol{\phi}_\text{R}^h).
\end{aligned}$$

We note that the first five expressions, common to both MFE and GFV, are often similar in size. As a gross measure of the effect of geometric projection and of the use of quadrature, we also report the two ratios

$$\text{ratio}_\text{proj} = \frac{\sum_{i=6}^{7} |\,\text{GFV}_i\,|}{\sum_{i=1}^{5} |\,\text{GFV}_i\,|}, \qquad \text{ratio}_\text{quad} = \frac{\sum_{i=8}^{9} |\,\text{GFV}_i\,|}{\sum_{i=1}^{5} |\,\text{GFV}_i\,|}.$$

We present three examples chosen to show the spectrum of possibilities in terms of the performance of the methods. Test Case 1 is an 'easy' case in which the geometric method performs relatively well. Test Case 2 has a narrow and severe dip in diffusivity located along the subdomain boundary and, consequently, the geometric method performs poorly, as might be expected for a problem in which the solution changes rapidly near the interface. Test Case 3 is based loosely on a real-world fusion problem and demonstrates one of our main conclusions, which is that the geometric method can perform poorly even when the solution is smooth near the interface. Note that the behaviour of the diffusivity function approaching the common interface on both sides has more impact on the accuracy of coupling than a discontinuity in the diffusivity across the interface.

4.1 *Verification of a posteriori estimate accuracy*

We begin with a problem for which we have manufactured the known solution

$$p(x, y) = \cos\left(\frac{\pi x}{2}\right) \cos\left(\frac{\pi y}{4}\right). \tag{4.1}$$

The diffusivity a is equal to 1 everywhere. The other solution components, the source term f and the boundary values g for the problem follow from (4.1). Since we know the true solution, we can compute the exact error terms (e, ψ) on the left in (3.10) and (3.11) directly and then compare with estimates of the quantities on the right computed using a numerical solution to the adjoint problem. In this situation, the most important issue for the accuracy of the estimates is the accuracy of the approximate adjoint solutions. As the grid for the adjoint problem is refined, the estimates become more accurate. That is, using the approximation to the adjoint problem, the estimated quantities $\sum \text{MFE}_i$ or $\sum \text{GFV}_i$ become closer to their true value, the error in the quantity of interest MFE $\sum(e, \psi)$ or GFV $\sum(e, \psi)$. Tables 1 and 2 show this using coarse and fine forward solutions.

TABLE 1 *The forward problem with solution* (4.1) *is run at* 10×10 *next to* 16×16. *The adjoint problem is run at several grids to show how the sum of terms approaches the direct calculation of* (e, ψ). *The adjoint data components* ψ_u *and* ψ_p *are constant everywhere and* $\psi_\xi = 0$

Adj. grid	MFE $\sum(e,\psi)$	$\sum$MFE$_i$	Ratio	GFV $\sum(e,\psi)$	$\sum$GFV$_i$	Ratio
$20 \times 20 : 32 \times 32$	1.96E−3	1.47E−3	.749	−1.00E−3	−1.50E−3	1.49
$40 \times 40 : 64 \times 64$	1.96E−3	1.84E−3	.937	−1.00E−3	−1.13E−3	1.12
$80 \times 80 : 128 \times 128$	1.96E−3	1.93E−3	.984	−1.00E−3	−1.03E−3	1.03
$160 \times 160 : 256 \times 256$	1.96E−3	1.96E−3	.996	−1.00E−3	−1.01E−3	1.01

TABLE 2 *The forward problem with solution* (4.1) *is run at* 40×40 *next to* 64×64. *The adjoint problem is run at several grids to show how the sum of terms approaches the direct calculation of* (e, ψ). *The adjoint data components* ψ_u *and* ψ_p *are constant everywhere and* $\psi_\xi = 0$

Adj. grid	MFE $\sum(e,\psi)$	$\sum$MFE$_i$	Ratio	GFV $\sum(e,\psi)$	$\sum$GFV$_i$	Ratio
$80 \times 80 : 128 \times 128$	1.23E−4	9.23E−5	0.750	−7.00E−5	−1.01E−4	1.44
$160 \times 160 : 256 \times 256$	1.23E−4	1.15E−4	0.937	−7.00E−5	−7.77E−5	1.11

4.2 *Convergence*

To compare the accuracy of the various approximations, we use the 2-norms

$$\|e_p\|_2 = \sqrt{\int_\Omega (p - p^h)^2}, \quad \|e_{u_x}\|_2 = \sqrt{\int_\Omega (u_x - u_x^h)^2},$$

$$\|e_{u_y}\|_2 = \sqrt{\int_\Omega (u_y - u_y^h)^2}, \quad \|e_\xi\|_2 = \sqrt{\int_\Gamma (\xi - \xi^h)^2}.$$

We use the manufactured solution from the previous section ($a = 1$ and p is given by (4.1)). We compare the 2-norm errors of the finite element and geometric finite volume methods on a sequence of grids in order to assess the convergence rate. The coarsest grid is 10×10 next to 16×16 and the number of cells in each dimension is doubled with each refinement.

The results in Tables 3–6 show that the convergence rate for the geometric finite volume deteriorates for the u_x, u_y and ξ components when the number of cells along the fine side of the interface is not an integer multiple of the number of cells along the coarse side of the interface. When the test is repeated with a grid starting at 8×8 next to 16×16, the convergence rates for the two methods are equal. The first-order convergence of p and u for the MFE is to be expected (Arbogast *et al.*, 2000).

4.3 *Test Case* 1

In the next problem, we explore accuracy for a solution that is not changing rapidly near the interface. We find that the use of geometric projections does not lead to significant effects on accuracy. We let the diffusivity a be 1 in both Ω_{L} and Ω_{R} and use the manufactured solution given by (4.1). The grid for the forward problem is 20×20 next to 32×32. The adjoint grid is 80×80 next to 128×128 and the adjoint datum are a nonzero constant for ψ_{u_x}, ψ_{u_y} and ψ_p, while $\psi_\xi = 0$.

TABLE 3 *Convergence of solution component p, indicating a rate of $\mathcal{O}(h)$*

Grid	MFE $\|e_p\|$	MFE ratio	GFV $\|e_p\|$	GFV ratio
$10 \times 10 : 16 \times 16$	1.20E−01	N/A	1.20E−01	N/A
$20 \times 20 : 32 \times 32$	5.98E−02	2.00	5.98E−02	2.00
$40 \times 40 : 64 \times 64$	2.99E−02	2.00	2.99E−02	2.00
$80 \times 80 : 128 \times 128$	1.49E−02	2.00	1.49E−02	2.00
$160 \times 160 : 256 \times 256$	7.47E−03	2.00	7.47E−03	2.00

TABLE 4 *Convergence of solution component u_x, indicating a rate of about $\mathcal{O}(h)$*

Grid	MFE $\|e_{u_x}\|$	MFE ratio	GFV $\|e_{u_x}\|$	GFV ratio
$10 \times 10 : 16 \times 16$	8.49E−02	N/A	8.63E−02	N/A
$20 \times 20 : 32 \times 32$	4.21E−02	2.02	4.26E−02	2.02
$40 \times 40 : 64 \times 64$	2.10E−02	2.00	2.14E−02	1.99
$80 \times 80 : 128 \times 128$	1.05E−02	2.00	1.09E−02	1.97
$160 \times 160 : 256 \times 256$	5.25E−03	2.00	5.63E−03	1.93

TABLE 5 *Convergence of solution component u_y, indicating a rate of $\mathcal{O}(h)$ for MFE but less for GFV*

Grid	MFE $\|e_{u_y}\|$	MFE ratio	GFV $\|e_{u_y}\|$	GFV ratio
$10 \times 10 : 16 \times 16$	8.41E−02	N/A	8.59E−02	N/A
$20 \times 20 : 32 \times 32$	4.20E−02	2.00	4.39E−02	1.96
$40 \times 40 : 64 \times 64$	2.10E−02	2.00	2.29E−02	1.92
$80 \times 80 : 128 \times 128$	1.05E−02	2.00	1.23E−02	1.86
$160 \times 160 : 256 \times 256$	5.25E−03	2.00	6.94E−03	1.77

TABLE 6 *Convergence of solution component ξ, indicating a rate of $\mathcal{O}(h^2)$ for MFE but only $\mathcal{O}(h)$ for GFV*

Grid	MFE $\|e_\xi\|$	MFE ratio	GFV $\|e_\xi\|$	GFV ratio
$10 \times 10 : 16 \times 16$	7.53e−03	N/A	6.11e−03	N/A
$20 \times 20 : 32 \times 32$	1.89e−03	3.99	1.79e−03	3.42
$40 \times 40 : 64 \times 64$	4.72e−04	4.00	6.37e−04	2.80
$80 \times 80 : 128 \times 128$	1.18e−04	4.00	2.77e−04	2.30
$160 \times 160 : 256 \times 256$	2.95e−05	4.00	1.33e−04	2.09

We list the error contributions in Table 7. For the geometric approach, we list results for both constant and linear extrapolation. The results show that the projection error for linear extrapolation is only about one quarter of the residual error, while the projection error for constant extrapolation is much larger. Figure 5 shows the solution components for the finite element case. The geometric finite volume solutions are very similar. Figure 6 shows the adjoint solution components.

TABLE 7 *Error terms for Test Case* 1. *The forward grid is* 20×20 *next to* 32×32. *The adjoint grid is* 80×80 *next to* 128×128

	Term	MFE	GFV (linear)	GFV (constant)
1	$(\boldsymbol{R}_{\boldsymbol{u}_\mathrm{L}}, \boldsymbol{\phi}_\mathrm{L}^h - \Pi_\mathrm{L}^h \boldsymbol{\phi}_\mathrm{L}^h)$	−1.6E−4	−1.6E−4	−1.5E−4
2	$(\boldsymbol{R}_{\boldsymbol{u}_\mathrm{R}}, \boldsymbol{\phi}_\mathrm{R}^h - \Pi_\mathrm{R}^h \boldsymbol{\phi}_\mathrm{R}^h)$	−6.1E−5	−6.1E−5	−6.1E−5
3	$(R_{p_\mathrm{L}}, \zeta_\mathrm{L}^h - P_\mathrm{L}^h \zeta_\mathrm{L}^h)$	4.9E−4	4.9E−4	4.9E−4
4	$(R_{p_\mathrm{R}}, \zeta_\mathrm{R}^h - P_\mathrm{R}^h \zeta_\mathrm{R}^h)$	1.9E−4	1.9E−4	1.9E−4
5	$\langle R_\xi, \beta^h - Z_h \beta^h \rangle_{\Gamma_\mathrm{I}}$	4.2E−8	−1.3E−6	1.0E−5
6	$\langle P_{\mathrm{R}\to\mathrm{L}}(p_\mathrm{R}^h) - \xi^h, \boldsymbol{n} \cdot \Pi_\mathrm{L}^h \boldsymbol{\phi}_\mathrm{L}^h \rangle_{\Gamma_\mathrm{I}}$	N/A	2.0E−4	1.7E−4
7	$\langle \boldsymbol{n} \cdot \boldsymbol{u}_\mathrm{L}^h - P_{\mathrm{L}\to\mathrm{R}}(p_\mathrm{L}^h), Z^h \beta^h \rangle_{\Gamma_\mathrm{I}}$	N/A	2.2E−5	3.9E−3
8	$\mathscr{Q}\mathscr{E}_{\boldsymbol{u}_\mathrm{L}}(\Pi_\mathrm{L}^h \boldsymbol{\phi}_\mathrm{L}^h)$	N/A	−7.1E−4	−7.0E−4
9	$\mathrm{QE}_{\boldsymbol{u}_\mathrm{R}}(\Pi_\mathrm{R}^h \boldsymbol{\phi}_\mathrm{R}^h)$	N/A	−2.8E−4	2.7E−4
	Total	4.6E−4	−3.0E−4	3.6E−3
	$\mathrm{ratio}_{\mathrm{proj}}$	N/A	.25	4.5
	$\mathrm{ratio}_{\mathrm{quad}}$	N/A	1.1	1.1

4.4 *Test Case* 2

The next test problem presents a more difficult solution for which the geometric projection error is by far the largest source of error. The grid is 40×40 next to 64×64 and the boundary conditions are $g = 0$ on both subdomains. Figure 7 shows profiles of the source and diffusivity, while Fig. 8 shows the adjoint data.[1]

Because the source is large but the diffusivity is small along the interface, the solution changes rapidly near this region. This leads to relatively large errors near the interface for the geometric finite volume method. When the adjoint data is concentrated near the interface, the relative size of these errors is revealed. Table 8 lists the error terms. For this particular example problem, and this particular error measure, the error due to geometric projection is nearly 80 times the total error associated with the residuals. Figure 9 shows the solution components for the finite element case, Fig. 10 shows the solution components for the geometric finite volume case and Fig. 11 shows the adjoint solution.

4.5 *Test Case* 3

In our final example, we examine a problem that places only one cell in the x direction in one of the subdomains. Such a grid is only appropriate if the solution in that subdomain is essentially one-dimensional and varies only parallel to the interface. This situation arises in core–edge coupling in a tokamak fusion reactor.

We construct a problem with a solution that is very nearly one-dimensional in one subdomain and contains variation in the second dimension well away from the interface. The pressure component of

[1] The shapes in Figs 7 and 8 are based on a normalized Gaussian of the form $ae^{-(x-b)^2}/2c^2$. The parameter a is for normalization and is set to $a = 1/c\sqrt{2\pi}$. The parameter b determines the location of the peak and is set to zero to coincide with the interface. The parameter c determines the width of the peak and is set to $c = 0.2$. In the case of diffusivity the dip is produced using the function $10.3 - 10(ae^{-(x-b)^2}/2c^2)$.

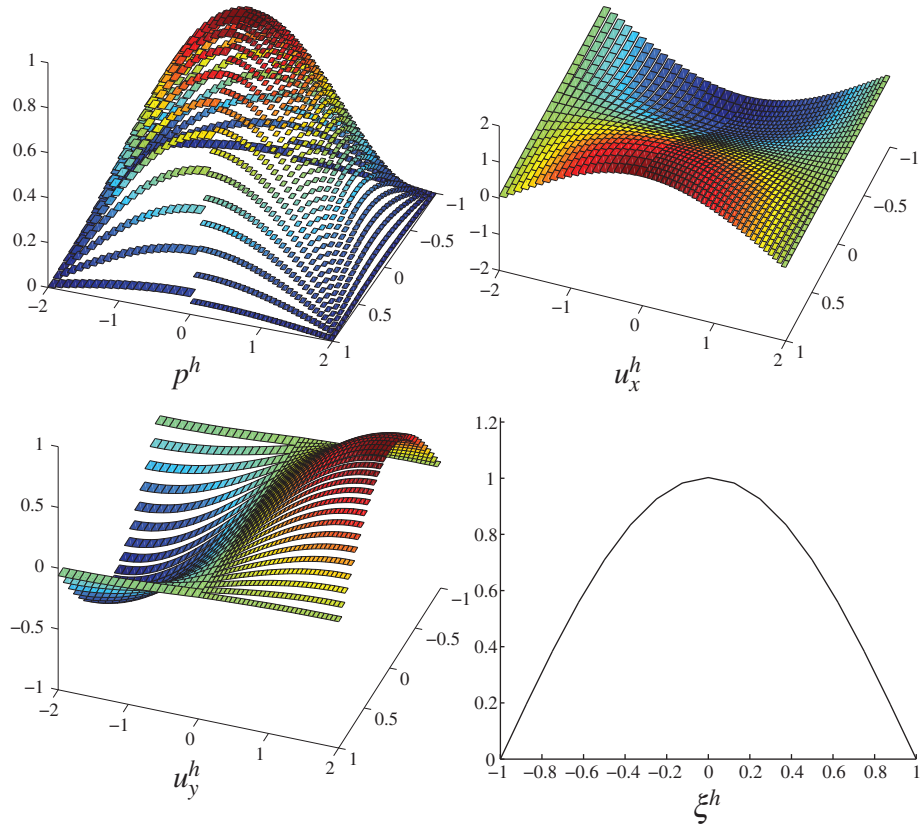

FIG. 5. Finite element solution components for Test Case 1.

the solution is

$$p(x,y) = \cos\left(\frac{\pi(y+2)}{8}\right) + 0.3\sin(\pi x)\left[\frac{1-\tanh(2(1.5-y))}{2}\right]. \tag{4.2}$$

The grid is 1×32 next to 32×32 and the boundary conditions are provided by evaluating the known solution at the outer domain boundaries. The source for the problem is computed by substituting the chosen solution into the PDE. The diffusivity a is 1 in both Ω_L and Ω_R. The adjoint data are concentrated in the finer subdomain and are shown in Fig. 12.

Table 9 lists the error terms. For this example problem, the contribution due to geometric projection with linear extrapolation is approximately 10 times the total contribution associated with the residuals, despite the fact that the solution is changing slowly near the interface. The projection contribution is much larger if constant extrapolation is used. Figure 13 shows the solution components for the finite element case, Fig. 14 shows the solution components for the geometric finite volume case and Fig. 15 shows the adjoint solution components.

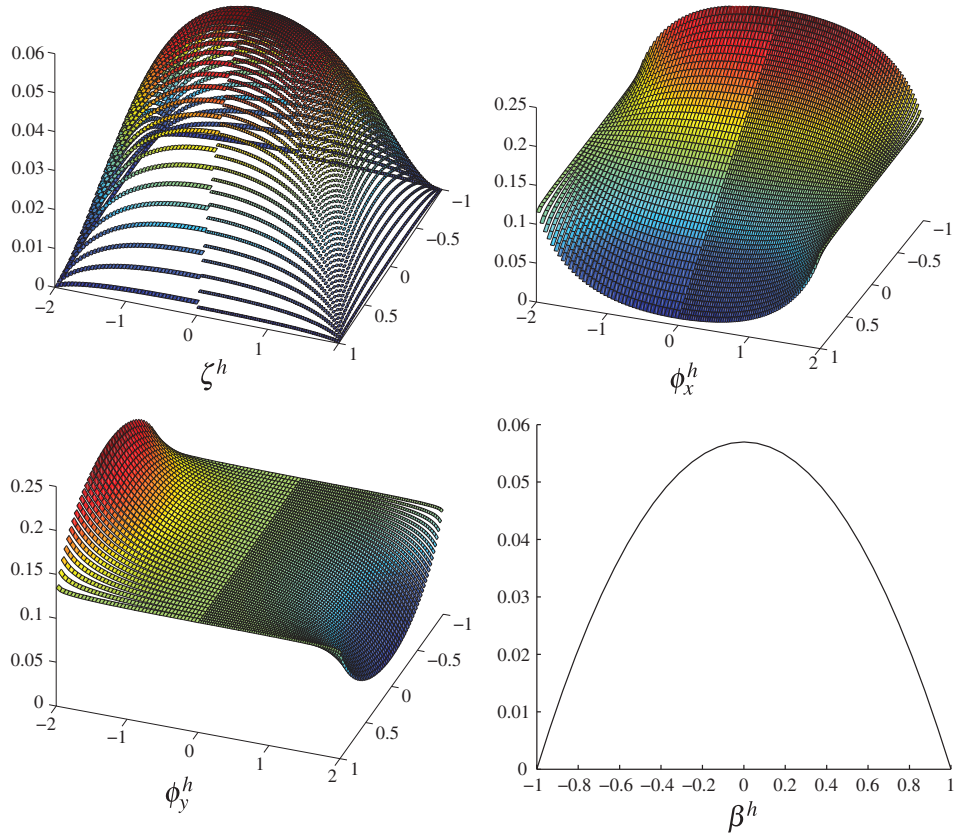

FIG. 6. Adjoint solution components for Test Case 1. Shown are plots for an adjoint solution using a 40×40 grid next to a 64×64 grid. A solution on a finer grid is used to compute the estimates.

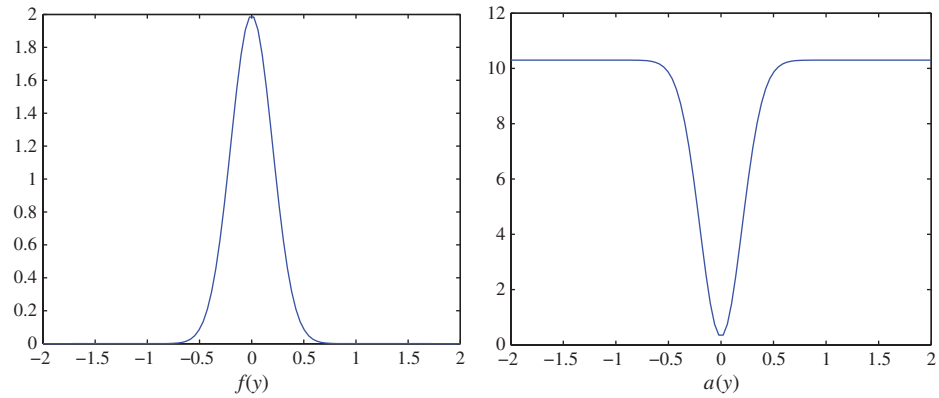

FIG. 7. Source f (left) and diffusivity a (right) profiles for Test Case 2. The plots are shown in one dimension since the source and diffusivity have no variation in the x direction.

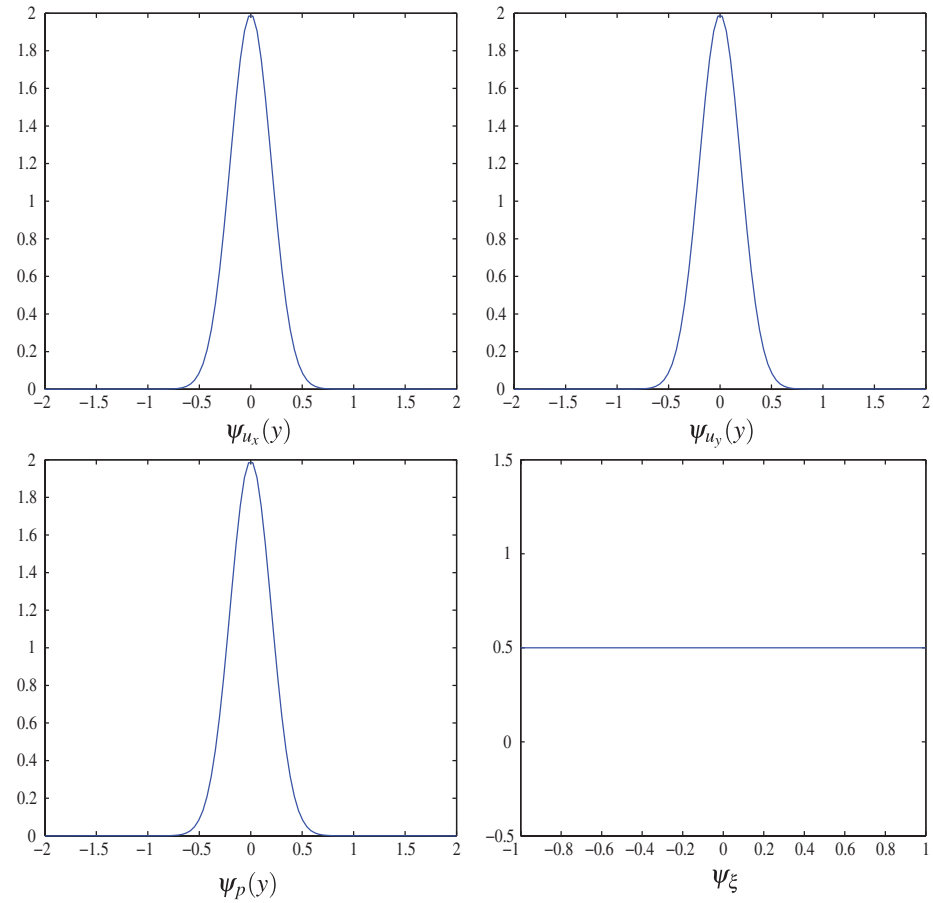

FIG. 8. Adjoint data profiles for Test Case 2. The plots of ψ_{u_x}, ψ_{u_y} and ψ_p are shown in one dimension because they have no variation in the x direction.

5. Iterative solvers and coupling strategies

In practice, an iterative solution of the coupled system is often employed. The specific choice of solution method is often constrained by certain computational logistics, such as the state of existing codes and data structures. We briefly discuss some aspects of iterative solution. The primary goal is to show that iterative solution strategies applied to systems like (2.10) can also be applied to systems like (2.7) without large changes to the computational structure. We do not discuss the convergence of iterative solvers.

5.1 *Iteration on the primary variable*

A common iterative technique for the geometric finite volume method (2.10) is to start with an initial guess $(p_{\mathrm{L}}^0, p_{\mathrm{R}}^0)$ and proceed with the iteration

$$\begin{bmatrix} A_{\mathrm{L}} & 0 \\ 0 & A_{\mathrm{R}} \end{bmatrix} \begin{bmatrix} p_{\mathrm{L}}^{i+1} \\ p_{\mathrm{R}}^{i+1} \end{bmatrix} = \begin{bmatrix} F_{\mathrm{L}} \\ F_{\mathrm{R}} \end{bmatrix} - \begin{bmatrix} 0 & C_D \\ C_N & 0 \end{bmatrix} \begin{bmatrix} p_{\mathrm{L}}^{i} \\ p_{\mathrm{R}}^{i} \end{bmatrix}, \quad i = 0, 1, 2, \ldots. \tag{5.1}$$

TABLE 8 *Error terms for Test Case* 2. *The forward grid is* 40×40 *next to* 64×64. *The adjoint grid is* 160×160 *next to* 256×256

	Term	MFE	GFV(linear)	GFV(constant)
1	$(\boldsymbol{R}_{\boldsymbol{u}_\mathrm{L}}, \boldsymbol{\phi}_\mathrm{L}^h - \Pi_\mathrm{L}^h \boldsymbol{\phi}_\mathrm{L}^h)$	1.6E−5	1.9E−5	2.4E−5
2	$(\boldsymbol{R}_{\boldsymbol{u}_\mathrm{R}}, \boldsymbol{\phi}_\mathrm{R}^h - \Pi_\mathrm{R}^h \boldsymbol{\phi}_\mathrm{R}^h)$	−2.6E−5	−2.6E−5	−2.5E−5
3	$(R_{p_\mathrm{L}}, \zeta_\mathrm{L}^h - P_\mathrm{L}^h \zeta_\mathrm{L}^h)$	−3.1E−5	−3.1E−5	−3.1E−5
4	$(R_{p_\mathrm{R}}, \zeta_\mathrm{R}^h - P_\mathrm{R}^h \zeta_\mathrm{R}^h)$	4.6E−5	4.6E−5	4.6E−5
5	$\langle R_\xi, \beta^h - Z_h \beta^h \rangle_{\Gamma_\mathrm{I}}$	4.8E−8	9.4E−6	2.6E−5
6	$\langle P_{\mathrm{R}\to\mathrm{L}}(p_\mathrm{R}^h) - \xi^h, \boldsymbol{n} \cdot \Pi_\mathrm{L}^h \boldsymbol{\phi}_\mathrm{L}^h \rangle_{\Gamma_\mathrm{I}}$	N/A	2.3E−3	2.7E−3
7	$\langle \boldsymbol{n} \cdot \boldsymbol{u}_\mathrm{L}^h - P_{\mathrm{L}\to\mathrm{R}}(p_\mathrm{L}^h), Z^h \beta^h \rangle_{\Gamma_\mathrm{I}}$	N/A	9.0E−4	8.4E−3
8	$\mathrm{QE}_{\boldsymbol{u}_\mathrm{L}}(\Pi_\mathrm{L}^h \boldsymbol{\phi}_\mathrm{L}^h)$	N/A	1.2E−3	1.2E−3
9	$\mathrm{QE}_{\boldsymbol{u}_\mathrm{L}}(\Pi_\mathrm{L}^h \boldsymbol{\phi}_\mathrm{L}^h)$	N/A	−2.4E−4	−2.5E−4
	total	5.1E−6	4.2E−3	1.2E−2
	$\mathrm{ratio}_{\mathrm{proj}}$	N/A	25	73
	$\mathrm{ratio}_{\mathrm{quad}}$	N/A	11	9.7

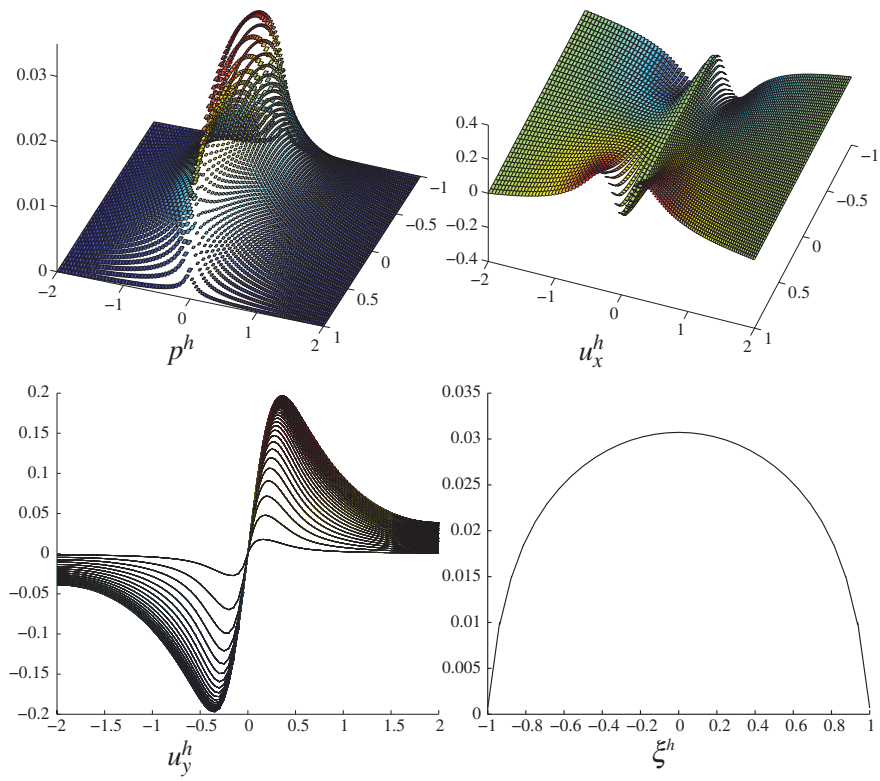

FIG. 9. Finite element solution components for Test Case 2. Zooming in reveals that u_y^h is smooth and continuous across the interface.

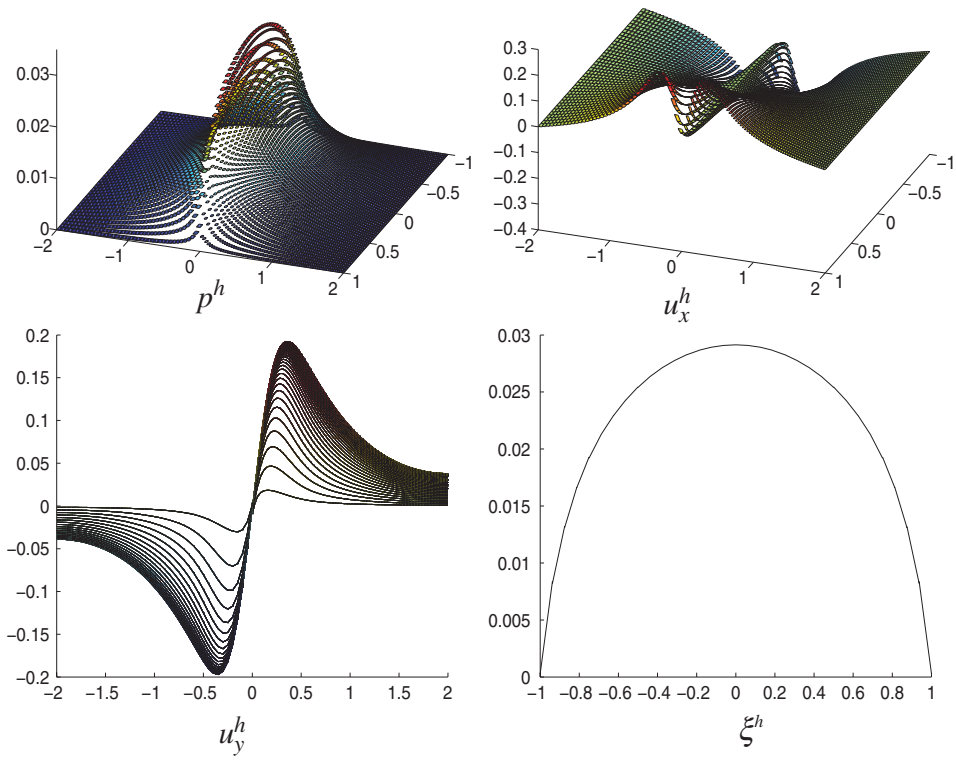

FIG. 10. Geometric finite volume solution components for Test Case 2. Zooming in reveals that u_y^h is discontinuous across the interface.

This iteration requires only the inversion of A_L and A_R, i.e., only single domain component solves. The application of C_D and C_N can be viewed as the coupling strategy, in which information is swapped between the subdomains.

It is possible to use an iteration of this type on the finite element system (2.7) as well. We must first reduce to a system in p by a preprocessing procedure. We first eliminate u_L and u_R, which results in

$$\begin{bmatrix} B_L^T M_L^{-1} B_L & 0 & -B_L^T M_L^{-1} C_L \\ 0 & B_R^T M_R^{-1} B_R & -B_R^T M_R^{-1} C_R \\ C_L^T M_L^{-1} B_L & C_R^T M_R^{-1} B_R & -(C_L^T M_L^{-1} C_L + C_R^T M_R^{-1} C_R) \end{bmatrix} \begin{bmatrix} p_L \\ p_R \\ \xi \end{bmatrix} = \begin{bmatrix} F_L + B_L^T M_L^{-1} D_L \\ F_R + B_R^T M_R^{-1} D_R \\ C_L^T M_L^{-1} D_L + C_R^T M_R^{-1} D_R \end{bmatrix}, \tag{5.2}$$

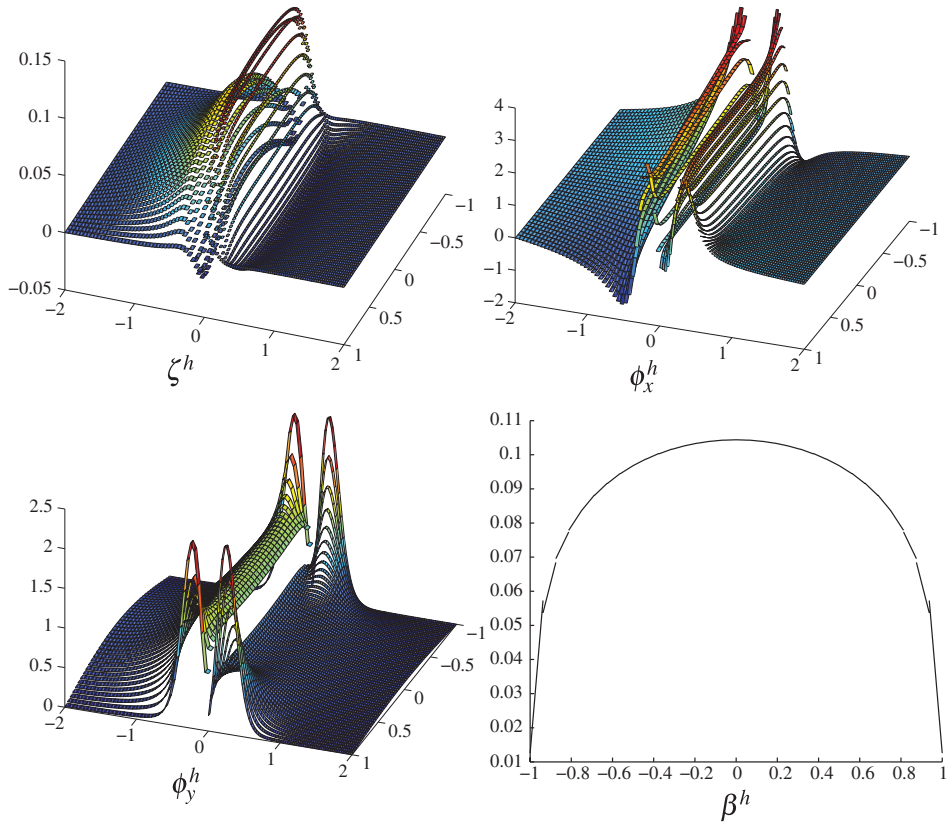

FIG. 11. Adjoint solution components for Test Case 2. Shown are plots for an adjoint solution using a 40×40 grid next to a 64×64 grid. A solution on a finer grid is used to compute the estimates.

which we write succinctly as

$$\begin{bmatrix} G_{\mathrm{L}} & 0 & -H_{\mathrm{L}} \\ 0 & G_{\mathrm{R}} & -H_{\mathrm{R}} \\ H_{\mathrm{L}}^{\mathrm{T}} & H_{\mathrm{R}}^{\mathrm{T}} & -(K_{\mathrm{L}}+K_{\mathrm{R}}) \end{bmatrix} \begin{bmatrix} p_{\mathrm{L}} \\ p_{\mathrm{R}} \\ \xi \end{bmatrix} = \begin{bmatrix} R_{\mathrm{L}} \\ R_{\mathrm{R}} \\ S_{\mathrm{L}}+S_{\mathrm{R}} \end{bmatrix}. \tag{5.3}$$

We then eliminate ξ to obtain

$$\begin{bmatrix} G_{\mathrm{L}} - H_{\mathrm{L}}(K_{\mathrm{L}}+K_{\mathrm{R}})^{-1}H_{\mathrm{L}}^{\mathrm{T}} & -H_{\mathrm{L}}(K_{\mathrm{L}}+K_{\mathrm{R}})^{-1}H_{\mathrm{R}}^{\mathrm{T}} \\ -H_{\mathrm{R}}(K_{\mathrm{L}}+K_{\mathrm{R}})^{-1}H_{\mathrm{L}}^{\mathrm{T}} & G_{\mathrm{R}} - H_{\mathrm{R}}(K_{\mathrm{L}}+K_{\mathrm{R}})^{-1}H_{\mathrm{R}}^{\mathrm{T}} \end{bmatrix} \begin{bmatrix} p_{\mathrm{L}} \\ p_{\mathrm{R}} \end{bmatrix}$$
$$= \begin{bmatrix} R_{\mathrm{L}} - H_{\mathrm{L}}(K_{\mathrm{L}}+K_{\mathrm{R}})^{-1}(S_{\mathrm{L}}+S_{\mathrm{R}}) \\ R_{\mathrm{R}} - H_{\mathrm{R}}(K_{\mathrm{L}}+K_{\mathrm{R}})^{-1}(S_{\mathrm{L}}+S_{\mathrm{R}}) \end{bmatrix}. \tag{5.4}$$

System (5.4) has the same structure as (2.10), so an iteration analogous to (5.1) can be applied. The stencil within the diagonal blocks of (5.4) is very close, but not identical, to the stencil of a single

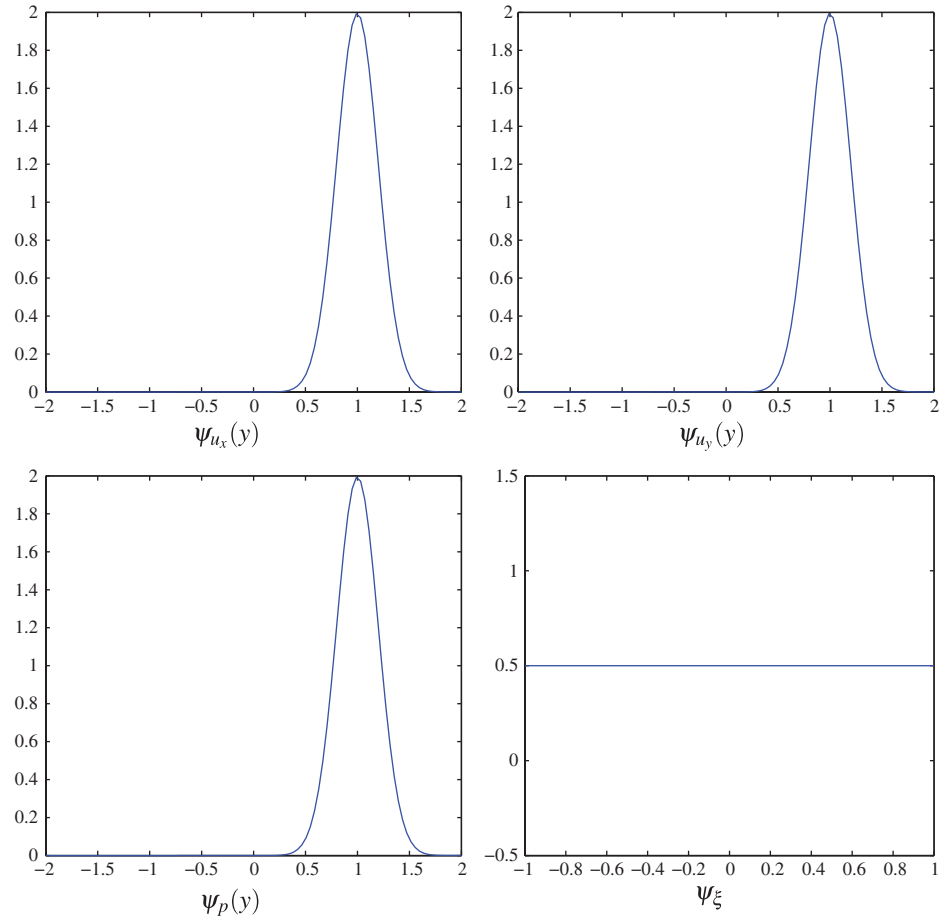

FIG. 12. Adjoint data profiles for Test Case 3. The plots of ψ_{u_x}, ψ_{u_y} and ψ_p are shown in one dimension because they have no variation in the x direction, and ψ_ξ is a one-dimensional function defined on the interface.

domain discretization. The difference occurs only in the stencil corresponding to cells touching the interface.

In some cases, e.g., the use of black-box single domain solvers, it is necessary to construct a system in which the diagonal blocks correspond exactly to single domain discretizations. If this is the case, the strategy of 'discretization-consistent interface conditions' provides a partial solution. In this strategy, the diagonal blocks are single domain discretizations, just as in (2.10). The off-diagonal blocks are populated by writing down both the Dirichlet and Neumann boundary condition equations for every cell touching the interface, rearranging those equations to isolate the boundary value terms and setting those terms equal to each other across the interface. If the cell ratio along the interface is integer, such as 4 next to 8, the resulting system is algebraically equivalent to (5.4). If the cell ratio is not an integer ratio, such as 5 next to 8, the equality of boundary value terms across the interface can only be enforced approximately and the resulting system is not exactly equivalent to (5.4). While a complete discussion of the implementation of discretization-consistent interface conditions is beyond the scope

TABLE 9 *Error terms for Test Case* 3. *The forward grid is* 1×32 *next to* 32×32. *The adjoint grid is* 128×128 *next to* 128×128

	Term	MFE	GFV (linear)	GFV (constant)
1	$(\boldsymbol{R}_{\boldsymbol{u}_\mathrm{L}}, \boldsymbol{\phi}_\mathrm{L}^h - \Pi_\mathrm{L}^h \boldsymbol{\phi}_\mathrm{L}^h)$	3.9E−9	6.8E−7	−1.5E−5
2	$(\boldsymbol{R}_{\boldsymbol{u}_\mathrm{R}}, \boldsymbol{\phi}_\mathrm{R}^h - \Pi_\mathrm{R}^h \boldsymbol{\phi}_\mathrm{R}^h)$	1.8E−5	1.8E−5	1.8E−5
3	$(R_{p_\mathrm{L}}, \zeta_\mathrm{L}^h - P_\mathrm{L}^h \zeta_\mathrm{L}^h)$	−4.0E−6	−4.0E−6	−4.0E−6
4	$(R_{p_\mathrm{R}}, \zeta_\mathrm{R}^h - P_\mathrm{R}^h \zeta_\mathrm{R}^h)$	7.2E−6	7.2E−6	7.2E−6
5	$\langle R_\xi, \beta^h - Z_h \beta^h \rangle_{\Gamma_\mathrm{I}}$	0	−3.8E−7	1.7E−5
6	$\langle P_{\mathrm{R}\to\mathrm{L}}(p_\mathrm{R}^h) - \xi^h, \boldsymbol{n} \cdot \Pi_\mathrm{L}^h \boldsymbol{\phi}_\mathrm{L}^h \rangle_{\Gamma_\mathrm{I}}$	N/A	1.5E−4	−6.4E−3
7	$\langle \boldsymbol{n} \cdot \boldsymbol{u}_\mathrm{L}^h - P_{\mathrm{L}\to\mathrm{R}}(p_\mathrm{L}^h), Z^h \beta^h \rangle_{\Gamma_\mathrm{I}}$	N/A	−6.8E−5	3.1E−3
8	$\mathscr{QE}_{\boldsymbol{u}_\mathrm{L}}(\Pi_\mathrm{L}^h \boldsymbol{\phi}_\mathrm{L}^h)$	N/A	−2.4E−5	2.5E−3
9	$\mathrm{QE}_{\boldsymbol{u}_\mathrm{R}}(\Pi_\mathrm{R}^h \boldsymbol{\phi}_\mathrm{R}^h)$	N/A	2.0E−5	1.9E−5
	Total	2.1E−5	1.0E−4	−8.0E−4
	$\mathrm{ratio}_{\mathrm{proj}}$	N/A	7.3	155
	$\mathrm{ratio}_{\mathrm{quad}}$	N/A	1.5	41

of this paper, it is worth consideration as an alternative to the full mortar method in cases where the computational structure is constrained by black-box single-domain solvers in combination with iteration on the primary variables. The concept of discretization-consistent interface conditions is similar to strategies employed in Farhat *et al.* (1998) and Edwards & Rogers (1998). We should remark that the former paper recommended against mortar methods for the fluid–structure interaction problem due to the lack of theory on optimal convergence and a need to invert a large interface matrix. However, for the problem considered in this paper, the mortar method does achieve optimal convergence. Moreover, we have presented several computational strategies that do not require inversion of an interface matrix.

5.2 *Iteration on interface variables*

An alternative iterative strategy (Glowinski & Wheeler, 1988) uses the interface variables as the primary variables. If we combine the u and p variables into the symbol ψ, then system (2.7) can be written as

$$\begin{bmatrix} \mathscr{A}_\mathrm{L} & 0 & \mathscr{C}_\mathrm{L} \\ 0 & \mathscr{A}_\mathrm{R} & \mathscr{C}_\mathrm{R} \\ \mathscr{C}_\mathrm{L}^\mathrm{T} & \mathscr{C}_\mathrm{R}^\mathrm{T} & 0 \end{bmatrix} \begin{bmatrix} \psi_\mathrm{L} \\ \psi_\mathrm{R} \\ \xi \end{bmatrix} = \begin{bmatrix} \mathscr{F}_\mathrm{L} \\ \mathscr{F}_\mathrm{R} \\ 0 \end{bmatrix}. \tag{5.5}$$

We eliminate ψ as

$$\psi_i = \mathscr{A}_i^{-1}(\mathscr{F}_i - \mathscr{C}_i \xi), \quad i = \mathrm{L}, \mathrm{R},$$

which gives the following system for ξ:

$$(\mathscr{C}_\mathrm{L}^\mathrm{T} \mathscr{A}_\mathrm{L}^{-1} \mathscr{C}_\mathrm{L} + \mathscr{C}_\mathrm{R}^\mathrm{T} \mathscr{A}_\mathrm{R}^{-1} \mathscr{C}_\mathrm{R}) \xi = (\mathscr{C}_\mathrm{L}^\mathrm{T} \mathscr{A}_\mathrm{L}^{-1} \mathscr{F}_\mathrm{L} + \mathscr{C}_\mathrm{R}^\mathrm{T} \mathscr{A}_\mathrm{R}^{-1} \mathscr{F}_\mathrm{R}). \tag{5.6}$$

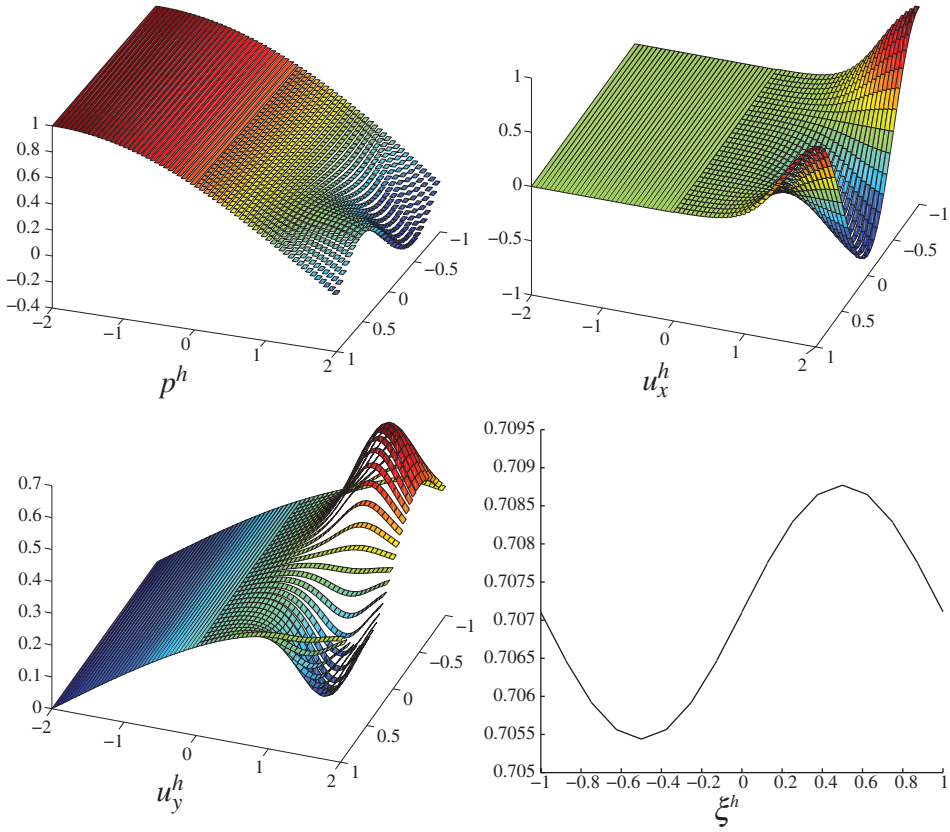

FIG. 13. Finite element solution components for Test Case 3.

If a Krylov method is applied to system (5.6), then only matrix–vector products involving the matrix on the left are required. Since this matrix contains $\mathscr{A}_{\mathrm{L}}^{-1}$ and $\mathscr{A}_{\mathrm{R}}^{-1}$, obtaining a matrix–vector product amounts to performing single-domain component solves. Once ξ is obtained, ψ is recovered as above.

In the setting of geometric coupling, we rewrite the geometric finite volume system as

$$\begin{bmatrix} A_{\mathrm{L}} & 0 & U_D & 0 \\ 0 & A_{\mathrm{R}} & 0 & U_N \\ 0 & E_D & -I & 0 \\ E_N & 0 & 0 & -I \end{bmatrix} \begin{bmatrix} p_{\mathrm{L}} \\ p_{\mathrm{R}} \\ D \\ N \end{bmatrix} = \begin{bmatrix} F_{\mathrm{L}} \\ F_{\mathrm{R}} \\ 0 \\ 0 \end{bmatrix}, \tag{5.7}$$

where A_{L} and A_{R} are single-domain finite volume systems, and the coupling strategy by which Dirichlet (D) and Neumann (N) data are provided by the opposite subdomain is defined by

$$E_N P_{\mathrm{L}} = N \quad \text{and} \quad E_D P_{\mathrm{R}} = D.$$

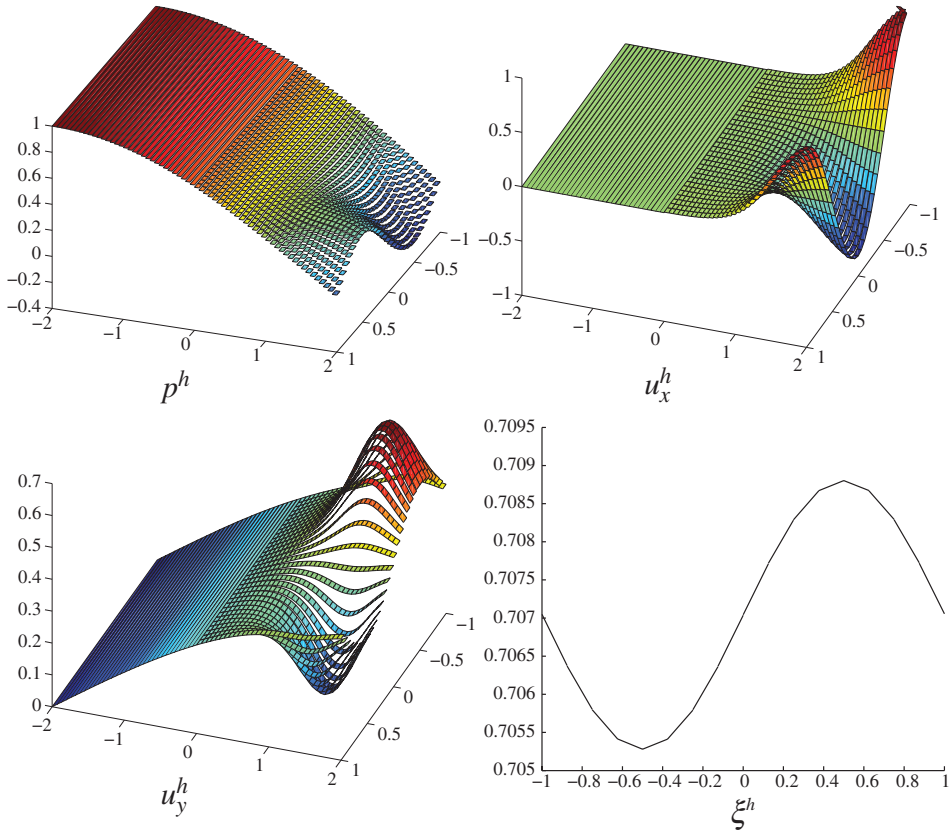

FIG. 14. Geometric finite volume solution components for Test Case 3 computed using linear extrapolation.

Eliminating D and N from system (5.7) gives

$$\begin{bmatrix} A_{\mathrm{L}} & U_D E_D \\ U_N E_N & A_{\mathrm{R}} \end{bmatrix} \begin{bmatrix} p_{\mathrm{L}} \\ p_{\mathrm{R}} \end{bmatrix} = \begin{bmatrix} F_{\mathrm{L}} \\ F_{\mathrm{R}} \end{bmatrix},$$

which is identical to (2.10). If instead we eliminate p_{L} and p_{R}, system (5.7) becomes

$$\begin{bmatrix} I & E_D A_{\mathrm{R}}^{-1} U_N \\ E_N A_{\mathrm{L}}^{-1} U_D & I \end{bmatrix} \begin{bmatrix} D \\ N \end{bmatrix} = \begin{bmatrix} E_D A_{\mathrm{R}}^{-1} F_{\mathrm{R}} \\ E_N A_{\mathrm{L}}^{-1} F_{\mathrm{L}} \end{bmatrix}, \tag{5.8}$$

which allows for an iteration of the form of (5.1) on the values D and N, from which the primary variables can be recovered. Solving (5.8) by iteration is analogous to solving (5.6) by iteration, and both require only component solves.

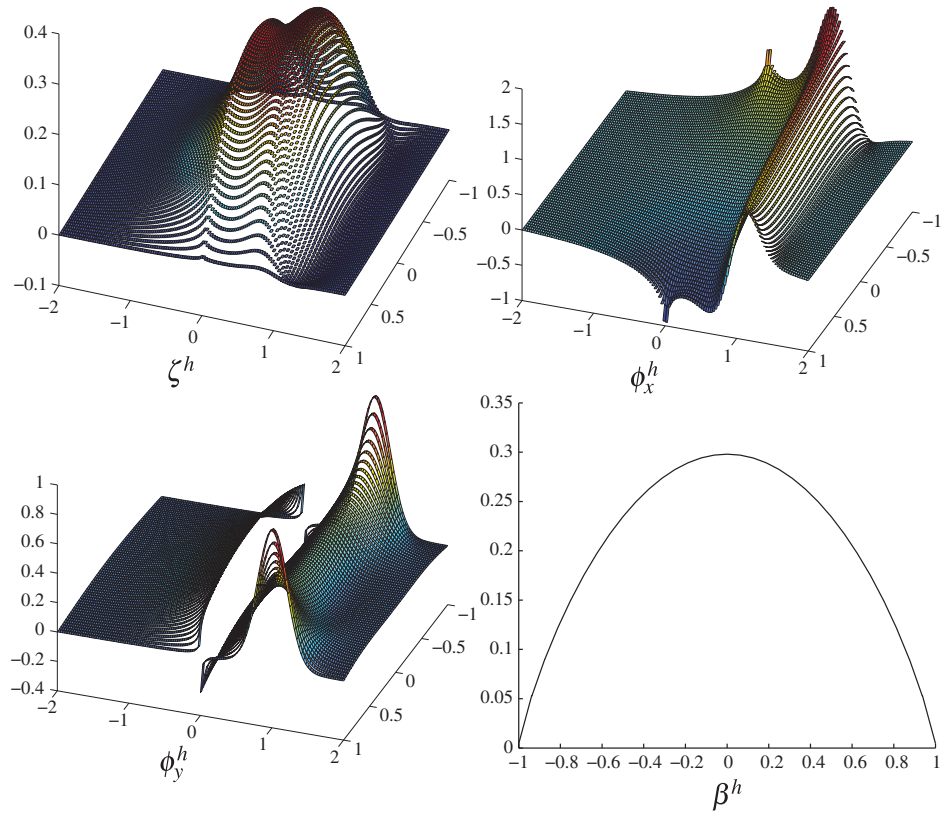

FIG. 15. Adjoint solution components for Test Case 3. These plots are the adjoint solution using 64×64 next to 64×64 meshes. The estimates were computed using a finer grid.

6. Conclusion

We compared the accuracy and performance of two numerical approaches to solving systems of PDEs. The equations were posed on adjoining domains which share a common boundary interface on which are imposed boundary conditions. We treated the important case of different and nonmatching meshes being used on the two domains. The first, widely used approach was based on a finite volume method employing *ad hoc* projections on the interface to relate approximations on the two domains. The second approach used the mathematically founded mortar mixed finite element method. To quantify the performance, we used a goal-oriented *a posteriori* error estimate that quantifies various aspects of discretization error to the overall error. The performance difference that we found may not be surprising in some cases. However, we believe that there is a perception in part of the scientific community concerned with multiphysics systems that if the solution is smooth near the interface, then it is not very important exactly how the coupling is accomplished. We found that, on the contrary, the error associated with *ad hoc* coupling approaches may be large in practical situations. The deterioration in accuracy was shown to be due mainly to incorrect transfer of information (or projection error) across the interface. Moreover, we also showed that mortar methods can be used with black-box component solves, thus permitting an efficient and practical implementation of the mortar coupling approach within legacy codes.

Funding

T.A.'s work was supported as part of the Center for Frontiers of Subsurface Energy Security, an Energy Frontier Research Center funded by the U.S. Department of Energy, Office of Science, Office of Basic Energy Sciences under Award Number DE-SC0001114. D.E.'s work was supported in part by the Defense Threat Reduction Agency (HDTRA1-09-1-0036), Department of Energy (DE-FG02-04ER25620, DE-FG02-05ER25699, DE-FC02-07ER54909, DE-SC0001724, DE-SC0005304, INL00120133), Idaho National Laboratory (00069249, 00115474), Lawrence Livermore National Laboratory (B584647, B590495), National Science Foundation (DMS-0107832, DMS-0715135, DGE-0221595003, MSPA-CSE-0434354, ECCS-0700559, DMS-1065046, DMS-1016268, DMS-FRG-1065046) and National Institutes of Health (#R01GM096192).

References

Arbogast, T., Cowsar, L. C., Wheeler, M. F. & Yotov, I. (2000) Mixed finite element methods on nonmatching multiblock grids. *SIAM J. Numer. Anal.*, **37**, 1295–1315.

Arbogast, T., Pencheva, G., Wheeler, M. F. & Yotov, I. (2007) A multiscale mortar mixed finite element method. *Multiscale Model. Simul.*, **6**, 319–346.

Becker, R. & Rannacher, R. (2001) An optimal control approach to *a posteriori* error estimation in finite element methods. *Acta Numer.*, **10**, 1–102.

Ben Belgacem, F. (2000) The mixed mortar finite element method for the incompressible Stokes problem: convergence analysis. *SIAM J. Numer. Anal.*, **37**, 1085–1100.

Bernardi, C., Maday, Y. & Patera, A. T. (1994) A new nonconforming approach to domain decomposition: the mortar element method. *Nonlinear Partial Differential Equations and their Applications*. UK: Longman Scientific and Technical.

Bernardi, C., Maday, Y. & Rapetti, F. (2005) Basics and some applications of the mortar element method. *GAMM-Mitt.*, **28**, 97–123.

Brezzi, F. & Fortin, M. (1991) *Mixed and Hybrid Finite Element Methods*. New York: Springer.

Cary, J. R., Candy, J., Cohen, R. H., Krasheninnikov, S., McCune, D. C., Estep, D. J., Larson, J., Malony, A. D., Worley, P. H., Carlsson, J. A., Hakim, A. H., Hamill, P., Kruger, S., Mia, M., Muzsala, S., Pletzer, A., Shasharina, S., Wade-Stein, D., Wang, N., Balay, S., McInnes, L., Zhang, H., Casper, T., Diachin, L., Epperly, T., Rognlien, T. D., Fahey, M. R., Cobb, J., Morris, A., Shende, S., Hammett, G. W., Indireshkumar, K., Stotler, D. & Yu Pigarovd, A. (2008) First results from core–edge parallel composition in the facets project. *J. Phys. Conf. Ser.*, **125**. Fourth Annual Scientific Discovery Through Advanced Computing Conference (SciDAC 2008).

Cary, J. R., Hakim, A., Miah, M., Kruger, S., Pletzer, A., Shasharina, S., Vadlamani, S., Cohen, R., Epperly, T., Rognlien, T., Pankin, A., Groebner, R., Balay, S., McInnes, L. & Zhang, H. (2010) Facets—a framework for parallel coupling of fusion components. *The 18th Euromicro International Conference on Parallel, Distributed and Network-Based Computing*. Pisa, Italy: IEEE, pp. 435–442.

Edwards, G. & Rogers, C. (1998) Finite volume discretization with imposed flux continuity for the general tensor pressure equation. *Comput. Geosci.*, **2**, 259–290.

Estep, D., Larson, M. G. & Williams, R. D. (2000) Estimating the error of numerical solutions of systems of reaction–diffusion equations. *Mem. Amer. Math. Soc.*, **146**, viii+109.

Estep, D., Pernice, M., Pham, D., Tavener, S. & Wang, H. (2009a) *A posteriori* analysis of a cell-centered finite volume method for semilinear elliptic problems. *J. Comput. Appl. Math.*, **233**.

Estep, D., Tavener, S. & Wildey, T. (2008) *A posteriori* analysis and improved accuracy for an operator decomposition solution of a conjugate heat transfer problem. *SIAM J. Numer. Anal.*, **46**, 2068–2089.

Estep, D., Tavener, S. & Wildey, T. (2009b) *A posteriori* error analysis for a transient conjugate heat transfer problem. *Fin. El. Anal. Design*, **45**, 263–271.

ESTEP, D., TAVENER, S. & WILDEY, T. (2010) *A posteriori* error estimation and adaptive mesh refinement for a multi-discretization operator decomposition approach to fluid-solid heat transfer. *J. Comput. Phys.*, **229**, 4143–4158.

FARHAT, C. M. L. & LETALLEC, P. (1998) Load and motion transfer algorithms for fluid/ structure interaction problems with non-matching discrete interfaces: momentum and energy conservation, optimal discretization and application to aeroelasticity. *Comput. Methods Appl. Mech. Engrg.*, **157**, 95–114.

GAIFFE, S., GLOWINSKI, R. & MASSON, R. (2002) Domain decomposition and splitting methods for mortar mixed finite element approximations to parabolic equations. *Numer. Math.*, **93**, 53–75.

GANIS, B. & YOTOV, I. (2009) Implementation of a mortar mixed finite element method using a multiscale flux basis. *Comp. Meth. Appl. Mech. Engng.*, **198**, 3989–3998.

GILES, M. B. & SULI, E. (2002) Adjoint methods for PDEs: *a posteriori* error analysis and postprocessing by duality. *Acta Numer.*, **11**, 145–236.

GLOWINSKI, R. & WHEELER, M. F. (1988) Domain decomposition and mixed finite element methods for elliptic problems. *First International Symposium on Domain Decomposition Methods for Partial Differential Equations* (R. Glowinski, G. H. Golub, G. A. Meurant & J. Periaux eds). Philadelphia: SIAM, pp. 144–172.

HANSBRO, P. & LARSON, M. G. (2011) *A posteriori* error estimates for continuous/discontinuous Galerkin approximations of the Kirchhoff–Love plate. *Comp. Meth. Appl. Mech. Engng.*, **200**, 3289–3295.

PENCHEVA, G., VOHRALIK, M., WHEELER, M. & WILDEY, T. (2013) Robust *a posteriori* error control and adaptivity for multiscale, multinumerics, and mortar coupling. *SIAM J. Numer. Anal.*, **51**, 526–554.

QUARTERONI, A., PASQUARELLI, F. & VALLI, A. (1992) Heterogeneous domain decomposition: principles, algorithms, applications. *Fifth International Symposium on Domain Decomposition Methods for Partial Differential Equations*. Philadelphia: SIAM, pp. 129–150.

ROBERTS, J. E. & THOMAS, J. (1991) Mixed and hybrid methods. *Handbook of Numerical Analysis*. Amsterdam: Elsevier, pp. 523–639.

RUSSELL, T. & WHEELER, M. F. (1983) Finite element and finite difference methods for continuous flows in porous media. *The Mathematics of Reservoir Simulation* (R. E. Ewing ed.). Philadelphia: SIAM, pp. 35–106.

WEISER, A. & WHEELER, M. F. (1988) On convergence of block-centered finite differences for elliptic problems. *SIAM J. Numer. Anal.*, **25**, 351–375.

WHEELER, M. F. & YOTOV, I. (2005) *A posteriori* error estimates for the mortar mixed finite element method. *SIAM J. Numer. Anal.*, **43**, 1021–1042.